15 July 2014

Volatility basis-set approach simulation of organic aerosol formation in East Asia: implications for anthropogenic-biogenic interaction and controllable amounts

H. Matsui, [1] M. Koike, [2] Y. Kondo, [2] A. Takami, [3]

J. D. Fast, [4] Y. Kanaya, [1] and M. Takigawa [1]

[1] Research Institute for Global Change, Japan Agency for Marine-Earth Science and Technology, Kanagawa, Japan

[2] Department of Earth and Planetary Science, Graduate School of Science, University of Tokyo, Tokyo, Japan

[3] National Institute for Environmental Studies, Ibaraki, Japan

[4] Pacific Northwest National Laboratory, Richland, Washington, USA.

Short title: MATSUI ET AL.: VBS OA SIMULATION IN EAST ASIA

Correspondence to: H. Matsui (matsui@jamstec.go.jp)

Submitted to Atmospheric Chemistry and Physics: 14 February, 2014

Revised following reviewer's comments: 15 July 2014

Abstract

Organic aerosol (OA) simulations using the volatility basis-set approach were made for East Asia and its outflow region. Model simulations were evaluated through comparisons with OA measured by aerosol mass spectrometers in and around Tokyo (at Komaba and Kisai in summer 2003 and 2004) and over the outflow region in East Asia (at Fukue and Hedo in spring 2009). The simulations with aging processes of organic vapors reasonably well reproduced mass concentrations, temporal variations, and formation efficiency of observed OA at all sites. As OA mass was severely underestimated in the simulations without the aging processes, the oxidations of organic vapors are essential for reasonable OA simulations over East Asia. By considering the aging processes, simulated OA concentrations increased from 0.24 to 1.28 μg m^{-3} in the boundary layer over the whole of East Asia. OA formed from the interaction of anthropogenic and biogenic sources was also enhanced by the aging processes. The fraction of controllable OA was estimated to be 87 % of total OA over the whole of East Asia, showing that most of the OA in our simulations formed anthropogenically (from controllable combustion sources). Even a large portion of biogenic secondary OA (78 % of biogenic secondary OA) was formed through the influence of anthropogenic sources. These fractions were higher than the fraction of anthropogenic emissions. An important reason for these higher controllable fractions was higher oxidant concentrations and resulting faster oxidation rates of OA precursors by considering anthropogenic sources. Both the amounts (from 0.18 to 1.12 μg m^{-3}) and the fraction (from 75 % to 87 %) of controllable OA were increased by aging processes of organic vapors over East Asia.

1. Introduction

Organic aerosol (OA) accounts for a significant mass fraction of the submicron aerosols in the atmosphere (Kanakidou et al., 2005; Zhang et al., 2007), and it influences the Earth's climate both directly (by scattering/absorbing of solar radiation) and indirectly (by modifying cloud microphysical properties) (Hallquist et al., 2009). OA is directly emitted from fossil fuel combustion, biomass burning, and other sources (primary organic aerosol, POA) or formed through the oxidation of thousands of volatile organic compounds (VOCs) in the atmosphere (secondary organic aerosol, SOA). Recent studies show that SOA accounts for a large fraction of OA globally (e.g., Kanakidou et al., 2005; Goldstein and Galbally, 2007; Zhang et al., 2007; de Gouw and Jimenez, 2009). However, as SOA formation processes are very complicated, estimates of the SOA burden in the atmosphere and its impact on climate and human health remain highly uncertain compared with those of other aerosols such as inorganic species (Hallquist et al., 2009). The current estimation of global SOA formation rate is about 30 – 450 Tg yr^{-1} (Hallquist et al., 2009; Heald et al., 2010; Spracklen et al., 2011).

In the traditional OA models, the mass concentrations of SOA produced from individual parent VOCs (for example, isoprene and terpenes for biogenic VOCs, and benzene, toluene and xylene for anthropogenic VOCs) are calculated with two mass-based yield coefficients and two partitioning coefficients which are estimated by fitting of laboratory experimental results (two-product approach) (Odum et al., 1996, 1997). Using these coefficients various global- and regional-scale simulations have been made (e.g., Chung and Seinfeld, 2002; Tsigaridis and Kanakidou, 2003, 2007; Heald et al., 2005, 2008), but they have underestimated observed OA and/or SOA concentrations and

formation rates in the atmosphere by approximately an order of magnitude, especially over urban regions (e.g., McKeen et al., 2007; Han et al., 2008; Matsui et al., 2009a).

More recently, a significant source of SOA was proposed by laboratory studies (e.g., Robinson et al., 2007), which found missing sources of semivolatile and intermediate volatility organic compounds (S/IVOCs) and the importance of chemical aging of S/IVOCs and VOCs in the atmosphere. Donahue et al. (2006) developed a new framework for OA modeling, the volatility basis set (VBS) approach. In the VBS, individual organic vapors are categorized to surrogate species with similar volatility, and their photochemical multigenerational oxidation and gas/particle partitioning processes are calculated. The VBS approach has recently been applied to both global- and regional-scale simulations (e.g., Lane et al., 2008a, 2008b; Farina et al., 2010; Pye and Seinfeld, 2010; Jathar et al., 2011). Improvement of the agreement between oxygenated OA (OOA, thought to be analogous to SOA) observed by aerosol mass spectrometers (AMS) and simulated SOA was reported for the air over Mexico City (Hodzic et al., 2010; Tsimpidi et al., 2010, 2011; Shrivastava et al., 2011), the United States (Ahmadov et al., 2012), and Europe (Fountoukis et al., 2011; Athanasopoulou et al., 2013).

East and Southeast Asia is one of the largest sources of aerosols in the world (e.g., Dentener et al., 2006; Bond et al., 2013). Many studies have reported impacts of Asian aerosols on regional and hemispherical scales (e.g., Ramanathan et al., 2001; Carmichael et al., 2003; Adhikary et al., 2010; Matsui et al., 2011a, 2011b, 2013a; Oshima et al., 2012, 2013). Several global and regional modeling studies have simulated and evaluated OA over East Asia (e.g., Heald et al., 2005; 2011; Han et al., 2008; Matsui et al., 2009a; Utembe et al., 2011; Mahmud and Barsanti, 2013). Most previous OA

92 simulation studies underestimated observed OA and SOA concentrations over the region.
93 For example, Utembe et al. (2011) evaluated their global OA simulations over the outflow
94 region in East Asia through the comparisons with OA measurements during the ACE-
95 Asia campaign. While their simulations reproduced the vertical profile of observed OA
96 mass concentrations, they underestimated absolute OA mass concentrations by a factor
97 of 5. Matsui et al. (2009a) made OA simulations over Tokyo urban area in July and
98 August 2003. The simulations reproduced absolute concentrations and their temporal
99 variations of observed NO_x, ozone (O_3), VOCs, and inorganic aerosols reasonably well,
100 but severely underestimated observed SOA (by a factor of 5) and OA concentrations (by
101 a factor of 2).

102 Few studies have focused on OA concentrations and their spatial distributions
103 over the whole of East and Southeast Asia and its outflow region (Han et al., 2008; Jiang
104 et al., 2012). They also underestimated observed OA and/or SOA concentrations over
105 China. As the VBS approach has a potential to explain realistic OA concentrations over
106 East and Southeast Asia, the application and evaluation of the VBS approach to the Asian
107 region is important for more quantitative understanding of OA concentrations and their
108 spatial distributions over the region.

109 The understanding on the interaction of anthropogenic and biogenic sources is
110 also very limited over the Asian region. Anthropogenic sources may substantially
111 influence biogenic SOA (BSOA) formation (e.g., Carlton et al., 2010; Hoyle et al., 2011;
112 Spracklen et al., 2011). The formation of BSOA is enhanced by anthropogenic POA,
113 NO_x, and VOCs because they increase the concentrations of precursor VOCs, the
114 oxidation rates of VOCs, and the particle-to-gas partitioning ratios of organic compounds

(e.g., Heald et al., 2008; Tsigaridis et al., 2006; Tsigaridis and Kanakidou, 2007). Carlton et al. (2010) estimated the effect of anthropogenic emissions on BSOA formation and demonstrated that more than 50 % of predicted BSOA concentrations were influenced by anthropogenic emissions in the eastern United States. Some global modeling studies estimated much higher contributions from enhanced BSOA (Tsigaridis et al., 2006; Hoyle et al., 2009; Spracklen et al., 2011). As both anthropogenic and biogenic emissions are very large over East and Southeast Asia, the interaction of anthropogenic and biogenic sources and the resulting enhancement of BSOA is very important and should be examined for the region. These understandings would be useful to estimate the past, current, and future OA concentrations and their regional and hemispherical climatic impacts.

The objective of this study is to understand OA concentrations and their spatial distributions over all of East and Southeast Asia and its outflow region with the interaction of anthropogenic and biogenic sources. We simulate OA concentrations over East Asia and its outflow region by using a VBS model we develop (Sect. 2), and evaluate the results through comparisons with AMS measurements conducted in and around Tokyo and over the outflow region in East Asia (Sect. 3 and 4). OA spatial distributions over East Asia are described with the importance of aging treatments in the VBS (Sect. 5.1.1). We also examine the interaction of anthropogenic and biogenic sources in OA formation processes, such as the enhancement of BSOA formation due to aging processes of anthropogenic S/IVOCs and VOCs (Sect. 5.1.3). Finally, we estimate the contribution of anthropogenically induced (controllable) OA over East Asia and the impact of aging treatments on it (Sect. 5.2). The abbreviations of organic vapors and aerosols used in

this study are summarized in Table 1.

2. Regional three-dimensional model

2.1. WRF-chem model

In this study, we use the Weather Research and Forecasting/Chemistry (WRF-chem) model with the MOSAIC aerosol module (version 3.4) (Skamarock et al., 2008; Grell et al., 2005; Fast et al., 2006; Zaveri et al., 2008), which has been used in our previous studies (Matsui et al., 2009b, 2010, 2011c, 2013b, 2013c), with modifications of the schemes related to organic aerosol formation (see Sect. 2.2). The chemical processes considered in the original WRF-chem model are emissions of gaseous and aerosol species, gas-phase chemistry (Zaveri and Peters, 1999), new particle formation (Wexler et al., 1994), dynamical gas-particle partitioning (condensation/evaporation) (Zaveri et al., 2005a, 2005b, 2008), Brownian coagulation (Jacobson et al., 1994), aqueous-phase chemistry for inorganic species (Fahey and Pandis, 2001), and dry and wet deposition (Easter et al., 2004). The mass (sulfate (SO_4), nitrate, ammonium, black carbon (BC), POA, dust, sodium, chloride, and aerosol water) and number concentrations of aerosol are explicitly calculated for the size range from 40 nm to 10 μm in 8 size bins. The meteorological and chemical process options adopted in this study are summarized in Table 2. More detailed descriptions of the WRF-chem/MOSAIC model are given elsewhere (Fast et al., 2006).

2.2. OA formation scheme (VBS)

The WRF-chem model was modified to consider OA formation processes using

161 the VBS approach (Fig. 1). Table 3 shows the summary of the OA formation scheme
162 developed in this study. Similar to previous studies (e.g., Lane et al., 2008a; Tsimpidi
163 et al., 2010, Shrivastava et al., 2011), this study uses 9 surrogate volatility species to
164 represent S/IVOCs with effective saturation concentrations (C*, saturation concentrations
165 at 300K) of 10^{-2}, 10^{-1}, 1, 10, 10^{2}, 10^{3}, 10^{4}, 10^{5}, and 10^{6} μg m^{-3}. Gas-phase chemistry is
166 represented by the SAPRC99 mechanism (Carter, 2000) with the formation of first-
167 generation oxidized VOCs (OVOCs) from the 9 lumped VOCs; alkanes (ALK4 and
168 ALK5), olefins (OLE1 and OLE2), aromatics (ARO1 and ARO2), isoprene (ISOP),
169 monoterpene (TERP), and sesquiterpene (SESQ). The mass yield of OVOCs from each
170 lumped VOC is calculated with the same NO_x-dependent 4-product basis fit (C* of 1, 10,
171 100, and 1000 μg m^{-3}) used in Tsimpidi et al. (2010). S/IVOCs and OVOCs are oxidized
172 to the surrogate species with an order of magnitude lower C* by OH radical with an
173 assumed rate constant of 1×10^{-11} cm^3 $molecule^{-1}$ s^{-1} (Fig. 1). The increase in SOA mass
174 due to the addition of an oxygen atom is taken into account, as described by Tsimpidi et
175 al. (2010): 7.5% increase for the reduction of volatility by one order of magnitude. The
176 enthalpy of vaporization is based on Tsimipidi et al. (2010) and Lane et al. (2008a): 64 –
177 112 kJ mol^{-1} for POA and 30 kJ mol^{-1} for SOA. Our scheme traces 53 surrogate vapor
178 species (9 for primary S/IVOCs, 8 for oxygenated S/IVOCs, and 36 for OVOCs) and the
179 corresponding 53 aerosol species for bulk aerosol mass concentrations. In this study,
180 we define oxidized POA (OPOA) as OA from oxygenated S/IVOCs, anthropogenic SOA
181 (ASOA) as OA from anthropogenic VOCs (ALK4, ALK5, OLE1, OLE2, ARO1, and
182 ARO2), and biogenic SOA (BSOA) as OA from biogenic VOCs (ISOP, TERP, and SESQ)
183 (Fig. 1).

184 The scheme assumes equilibrium between the vapor and particulate species.
185 Bulk equilibrium gas-particle partitioning is calculated with an iteration scheme of Schell
186 et al. (2001). The changes in size-resolved mass concentrations in 8 size bins are
187 calculated based on Koo et al. (2003) with the Kelvin effect. The fraction of total flux
188 of species *i* between gas and aerosol phases that condenses onto or evaporates from
189 aerosol size bin *k* ($f_{i,k}$) is given by
190
191 $$f_{i,k} = \frac{2\pi N_k d_k D_i F(C_i - C_i^{eq}\eta)}{\sum_k 2\pi N_k d_k D_i F(C_i - C_i^{eq}\eta)} \quad (1)$$
192
193 where N_k is the number concentrations in bin *k*, d_k is the mean diameter of bin *k*, D_i, C_i,
194 and C_i^{eq} are the diffusivity, bulk gas-phase concentration, and equilibrium concentration
195 at the particle surface of species *i*, respectively, *F* is the correction for non-continuum
196 effects which depends on the Knudsen number and the accommodation coefficient (0.1
197 is assumed), and η is the Kelvin effect correction. In our scheme, equation (1) is
198 calculated for individual VBS species (53 species), but all of the size-resolved
199 information is not directly used for the calculation of three-dimensional transport
200 processes to reduce computational cost. Only total OA (sum of all VBS species) is
201 transported with the size-resolved information, and individual VBS species are
202 transported with the information of bulk mass concentrations only (not size-resolved, we
203 assume all VBS species have the same size distribution). This treatment can reduce the
204 number of transport variables (therefore computational cost) by a factor of 4 compared
205 with the size-resolved treatment for all VBS species and by a factor of 3 compared with
206 the 4-bin scheme in Shrivastava et al. (2011) which was implemented in original WRF-

chem model (Table 3). Therefore, the scheme developed in this study is a detailed (9 species), size-resolved (for total OA), and computationally efficient VBS scheme.

In WRF-chem, interstitial (aerosol-phase) and in-cloud (cloud-phase) aerosols are treated separately for all aerosol species (5 inorganic species, BC, OA, and dust) and size bins to calculate in-cloud aerosol formation, regeneration, and wet removal processes. Therefore, OA size distribution is calculated separately for aerosol-phase and cloud-phase in our model. The model considers the increase in total OA (sum of all VBS species) through aerosol regeneration after cloud evaporation. Since the information of each VBS species is not calculated for in-cloud aerosols in our model, chemical composition (mass fraction of each VBS species) of regenerated OA is assumed to be that of interstitial OA at the same three-dimensional grid cell.

The emission factors of S/IVOCs and POA were assumed based on Shrivastava et al. (2011). In this study, we apply the factors for anthropogenic sources (Table 2 of Shrivastava et al. (2011)) to all the emission sources. The sum of all S/IVOCs and POA emissions is 7.5 times traditional POA emissions (Fig. 1), which is based on the rough estimate of the SVOC/POA ratio of 3 and the IVOC/SVOC ratio of 1.5 (or the IVOC/POA ratio of 4.5) in previous studies (Tsimpidi et al., 2010; Shrivastava et al., 2011). To make consistent aerosol number concentrations between traditional OA emissions and S/IVOCs/POA emissions, we assume particulate emissions (POA) for C* ranging from 10^{-2} to 1 μg m^{-3}, gas-phase emissions (S/IVOCs) for C* ranging from 10^{6} to 10^{2} μg m^{-3}, and the mixture of gas-phase and particulate emissions for C* of 10 μg m^{-3} (Fig. 1).

Dry deposition of organic vapors (S/IVOCs and OVOCs) is calculated by the scheme of Wesely (1989), which is used in the original WRF-chem/MOSAIC model. In

this study, the dry deposition velocity of HNO_3 is assumed for all the organic vapors, which is consistent with Ahmadov et al. (2012). Dry deposition of OA is calculated for each size bin with the scheme used in the original WRF-chem model (Binkowski and Shankar, 1995; Easter et al., 2004). In-cloud scavenging of organic vapors (S/IVOCs and OVOCs) is calculated by assuming aqueous-phase fraction of unity (all organic vapors are soluble). Below cloud scavenging of organic vapors is calculated by assuming the mass transfer rate of HNO_3 to rain given in Levine and Schwarz (1982). In-cloud and below cloud scavenging of OA is calculated for each size bin as calculated in the original WRF-chem model (Easter et al., 2004). A hygroscopicity value (κ) of 0.14, which is the value used in the original WRF-chem for POA, is assumed for all the OA species used in the VBS.

In our VBS model, oxidation processes are considered only for gaseous species, namely, homogenous aging by OH radical. Our model does not consider other processes, such as aqueous-phase reactions (e.g., Ervens et al., 2011; Liu et al., 2012), heterogeneous oxidation (e.g., George et al., 2007, 2008), oligomerization (e.g., Kalberer et al., 2004; Iinuma et al., 2004), and fragmentation (e.g., Jimenez et al., 2009; Kroll et al., 2009; Murphy et al., 2012). These processes could be important because they form OA from organic vapors and alter volatility and oxidation state (i.e., an atomic O/C ratio) of organic vapors and OA, leading to changes in OA concentrations. However, currently these processes have large uncertainties in reaction rates and products (Hallquist et al., 2009). Some recent studies developed two-dimensional VBS schemes (2D-VBS), in which both volatility and oxidation state were calculated considering functionalization and fragmentation (e.g., Jimenez et al., 2009; Donahue et al., 2011; Murphy et al., 2011, 2012;

Shrivastava et al., 2013). In Murphy et al. (2012), heterogeneous oxidation and aqueous-phase chemistry processes were also taken into account. They applied their one-dimensional (column) chemical transport model to Europe and showed that the simple one-dimensional (volatility only) VBS (1D-VBS) scheme reproduced observed OA mass concentrations and O/C ratios reasonably well and that the performance of the 1D-VBS scheme was not worse than that of their more complex 2D-VBS schemes, likely due to uncertainties in the understanding of SOA evolution in the atmosphere. Considering these uncertainties and computational costs of complex 2D-VBS schemes, we use a simpler 1D-VBS scheme in this study.

2.3. Uncertainties in the treatment of VBS model

To understand uncertainties of the simplicity in our VBS model, we conducted a sensitivity simulation without the simplicity. In this simulation, OA size distribution is calculated for each VBS species (53 species × 8 size bins). Aerosol-phase and cloud-phase aerosols and their size distributions are calculated separately for each VBS species. From the comparison between this sensitivity simulation including full representation of OA species and the base case simulation with the simplicity, the uncertainties in the estimation of SOA mass concentrations in the base simulation were estimated to be about 20% (as a total effect of OA formation, activation, and removal processes). The correlation coefficient (R^2) of SOA spatial distribution (at about 1 km) between the two simulations was 0.96, suggesting that the performance of OA distributions is good enough in the base case simulation.

Our VBS scheme has large uncertainties in the treatment of aging parameters,

276 emission factors, and dry and wet deposition of organic vapors, which could change
277 simulated OA concentrations considerably. In this study, the sensitivity of aging
278 coefficients is examined in Sect. 4.2 and 5.1.2. The uncertainties in emission factors
279 and the treatment of dry and wet deposition for organic vapors used in the VBS scheme
280 are described briefly here. The S/IVOCs-to-POA emission ratio of 7.5 used in this study
281 is a highly uncertain parameter. A sensitivity simulation with the increase in SVOC (C*
282 ranging from 10^3 to 10^{-2} μg m^{-3}) emissions by a factor of 2 enhanced total OA and SOA
283 concentrations by 25% and 45%, respectively, in our application over East Asia (period-
284 and domain-averaged values at an altitude of about 1 km). Another sensitivity
285 simulation with the increase in IVOC (C* ranging from 10^6 to 10^4 μg m^{-3}) emissions by
286 a factor of 2 enhanced total OA and SOA concentrations by 20% and 15%, respectively.
287 These results suggest OA concentrations are moderately sensitive to the treatment of
288 S/IVOC emissions over East Asia. OA concentrations are sensitive to the treatment of
289 dry deposition of organic vapors because a factor of 2 different velocities for S/IVOCs
290 and OVOCs lead to an increase/decrease in OA concentrations about 50% in our
291 application over East Asia. OA concentrations also have moderate sensitivity to the
292 treatment of wet deposition of S/IVOCs and OVOCs. OA concentrations were
293 increased by 25% in the simulation without wet deposition of S/IVOCs and OVOCs.
294
295 **3. Measurements and simulation setups**
296 In this study, we simulate OA formation both in and around Tokyo urban area
297 (Sect. 3.1) and over East Asia (Sect. 3.2). The purpose of the simulation in and around
298 Tokyo is to validate the VBS scheme over the region where meteorological fields,

299 emissions, and the concentrations of precursor gaseous species are relatively well known
300 (compared with over the Asian region). We used observed data during the Integrated
301 Measurement Program for Aerosol and oxidant Chemistry in Tokyo (IMPACT) campaign
302 (Takegawa et al., 2006a, 2006b; Kondo et al., 2006, 2007, 2008, 2010). OA mass
303 concentrations observed with an Aerodyne AMS and gaseous species such as O_3, OH,
304 and VOCs are available for the campaign period. These observation data can be used
305 not only to validate the simulations but also to constrain the parameters related to OA
306 formation such as precursor VOCs. The simulation over Asia is conducted to
307 understand the behavior of OA over all of East and Southeast Asia and its outflow region,
308 though there are uncertainties in emissions and limitations of validations especially for
309 precursor gases. OA mass concentrations (Aerodyne AMS) at two sites in Japan were
310 used to evaluate the simulations over the outflow regions from the Asian continent.
311
312 **3.1. Simulation in and around Tokyo (summer 2003 and 2004)**
313 We used OA mass concentrations observed by an Aerodyne AMS and gaseous
314 species of O_3 and VOCs at an urban area, Komaba (35.66°N, 139.67°E), Tokyo, in July
315 and August 2003 during the IMPACT-2 campaign and at a suburban site, Kisai (36.08°N,
316 139.55°E), Saitama, in July and August 2004 during the IMPACT-L campaign (Fig. 2a).
317 Details of the measurements are given elsewhere (Takegawa et al., 2005, 2006a, 2006b;
318 Kondo et al., 2006, 2007, 2008, 2010, Shirai et al., 2007; Kanaya et al., 2007).
319 The oxygenated and hydrocarbon-like OA concentrations (OOA and HOA) were
320 estimated by least-squares fits to the time series of OA using a linear combination of the
321 time series of AMS-derived signals at mass-to-charge (m/z) ratios 44 and 57 (Zhang et

al., 2005). Though there are some uncertainties in this method, the OOA/HOA concentrations derived from this method can be used as a proxy of SOA/POA concentrations because SOA and POA concentrations, which were estimated from the correlation of total OA with CO, correlated well with HOA and OOA with slopes of 0.88–1.36 (R^2 of 0.76 – 0.85) and 0.97–1.41 (R^2 of 0.65 – 0.85), respectively, during the IMPACT campaign (Takegawa et al., 2006a, 2006b; Kondo et al., 2007). We used observed HOA concentrations to constrain POA emissions and to simulate realistic POA concentrations by the model (see below). Observed OOA is used to validate simulated SOA (Sect. 4.1).

For the simulation in and around Tokyo, the horizontal grid spacings in the model domain are 27 km (outer domain) and 9 km (inner domain) (horizontal scale of 9 × 7 degrees, Fig. 2a), and there are 18 vertical levels from the surface to 100 hPa. The lowest layer is about 30 m in depth. The simulation periods are 17 July – 15 August 2003 during the IMPACT-2 campaign and 23 July – 15 August 2004 during the IMPACT-L campaign. The first 2 days of data were used for model spin-up. The National Centers for Environmental Prediction (NCEP) Final (FNL) Operational Global Analysis data were used for initial and boundary conditions and nudging (free troposphere only) of meteorological fields. We made two model simulations, with and without aging processes of organic vapors in the VBS.

We used anthropogenic emission inventories for 1998 at a horizontal resolution of 10 × 10 km^2 with seasonal and diurnal dependencies (Kannari et al., 2004). The detailed description of the inventories is given by Matsui et al. (2009a). We also used on-line biogenic emissions: the Model of Emissions of Gases and Aerosols from Nature

345 version 2 (MEGAN2) (Guenther et al., 2006). Using the same approach as described in
346 Matsui et al. (2009a), the emissions of aromatics (toluene and xylene) and POA were
347 increased or decreased over all the simulation domains (without modification of spatial
348 emission patterns) to achieve good agreement between observed and simulated mean
349 concentrations of these species at the Komaba site during the IMPACT-2 campaign:
350 ARO1 (toluene-like) and ARO2 (xylene-like) emissions were reduced by 50% and 30%,
351 respectively, and POA emissions were increased by 25%. As the simulations with these
352 modifications can reproduce mean concentrations of aromatics and POA during the
353 simulation period, at least at and around Komaba, we can robustly evaluate the
354 performance of OA formation processes. Note that the modifications of POA emissions
355 were applied to the simulations in and around Tokyo only. We do not use these
356 modifications in the simulations over East Asia (section 3.2).
357
358 **3.2. Simulation over East Asia (spring 2009)**
359 We used OA and sulfate mass concentrations observed with an Aerodyne AMS at
360 Fukue (32.75°N, 128.68°E) and Hedo (26.87°N, 128.25°E), Japan, in March and April
361 2009 during the Aerosol Radiative Forcing in East Asia (A-FORCE) aircraft campaign
362 (Oshima et al., 2012). As described by Takami et al. (2005, 2007), the collection
363 efficiency was assumed to be 0.5 at Fukue and 1.0 at Hedo. Details of the AMS
364 measurements at Fukue and Hedo are described by Takami et al. (2005, 2007). OA
365 measurements over the outflow regions in East Asia are limited and they are useful to
366 evaluate model simulations. The air parcels observed at Fukue and Hedo represent the
367 history of sources from wide areas over northern China and their histories during the

368 transport (e.g., Kondo et al., 2011; Matsui et al., 2013a), which suggests model
369 evaluations at these sites are suitable for overall validations of sources, transport, and
370 transformation of aerosols from the Asian continent to the Pacific. We also used BC
371 mass concentrations observed with the continuous soot monitoring system (COSMOS) to
372 evaluate primary aerosol at Fukue and Hedo (Kondo et al., 2011).

373 For the simulation over East Asia, the horizontal grid spacings for the model
374 domain are 180 km (outer domain) and 60 km (inner domain) (horizontal scale of 120 ×
375 60 degrees, Fig. 2b), and there are 26 vertical levels from the surface to 100 hPa. The
376 lowest layer is about 30 m in depth. The simulation period is 21 March – 26 April 2009
377 during the A-FORCE aircraft campaign. Statistics are calculated for 24 March – 26
378 April 2009 period. The NCEP-FNL data were used for initial and boundary conditions
379 and nudging (free troposphere only) of meteorological fields. Our previous simulations
380 using WRF-chem successfully reproduced meteorological fields due to synoptic-scale
381 meteorological variations and related transport and variation processes of aerosol mass
382 and number concentrations observed by both the aircraft and surface measurements
383 during the A-FORCE period (Matsui et al., 2013b, 2013c). Our previous simulation
384 using similar model settings also showed that observed precipitation and its spatial
385 distributions were generally reproduced by WRF during the simulation period (Oshima
386 et al., 2013). Table 4 shows the list of simulations over East Asia conducted in this study.

387 We used the anthropogenic and volcanic emission inventories of Streets et al.
388 (2003), which were also used in our previous studies (Matsui et al., 2013b, 2013c). SO_2
389 emissions from the Miyakejima volcano were modified based on measurements, as shown
390 by Matsui et al. (2013c). We also used daily biomass burning emissions from the Global

391 Fire Emissions Database version 3 (GFED3) (van der Werf et al., 2010), and on-line
392 biogenic emissions from MEGAN2. Sea salt and dust emissions from natural sources
393 are not considered in this study.

394 Anthropogenic POA (from fossil fuel and biofuel combustion) is emitted mostly
395 from China and India (Fig. 3a), while biomass burning POA is emitted mainly from
396 Southeast Asia and Siberia (Fig. 3b). Anthropogenic and biomass burning sources
397 account for 69 % and 31 % of total POA emissions, respectively. ARO1 (anthropogenic)
398 emissions are distributed over China, India, Southeast Asia, Japan, and South Korea (Fig.
399 3c). The main source regions of TERP (biogenic) are Southeast Asia and southern
400 China (Fig. 3d).

401

402 **4. Model results and evaluation**

403 **4.1. IMPACT campaign (Tokyo)**

404 Figures 4a and b show the time-series of O_3 and SOA at Kisai during the
405 IMPACT-L campaign (25 July – 15 August 2004). Simulated SOA is the sum of OPOA,
406 ASOA, and BSOA. Simulated concentrations in Sect. 4 are chosen from a grid cell
407 closest to each measurement site and are calculated for particles smaller than 1 μm in
408 diameter. The data at the lowest layer are chosen for the comparison with the surface
409 measurements. Meteorological conditions during the campaign are summarized by
410 Takegawa et al. (2006a). Northerly and easterly winds were dominant during 25 – 30
411 July, persistent southerly winds were dominant during 31 July – 9 August (associated
412 with a stable anticyclone located east of Tokyo), and the sea-land breeze circulation was
413 dominant during 10 – 14 August (associated with a stable anticyclone over Tokyo). Due

414 to these meteorological conditions, relatively fresh air was transported from the Tokyo
415 metropolitan area to Kisai by 9 August, which was the cause of relatively low O_3 and
416 SOA concentrations at Kisai. In contrast, stagnant and aged air was transported to Kisai
417 during 10 – 14 August, which enhanced both O_3 and SOA at Kisai through the
418 accumulation of pollutants.

419 The simulation reproduces the absolute concentrations and the diurnal and day-
420 to-day variations of observed O_3 and SOA concentrations reasonably well (Fig. 4 and
421 Table 5). In particular, the model reproduces the contrast between the early (25 July –
422 6 August, low concentrations) and the later (7 – 15 August, high concentrations)
423 simulation periods and the diurnal peak concentrations of both O_3 and SOA (Fig. 4). The
424 daytime peak concentrations of OH and HO_2 radicals are also reproduced within 50% at
425 Komaba during the IMPACT-L campaign in our simulations, though the concentrations
426 have large day-to-day variability: the median values of the daytime peak concentrations
427 of observed OH and HO_2 were 6.3×10^6 cm^{-3} and 5.7 pptv, respectively (Kanaya et al.,
428 2007), and those of simulated OH and HO_2 were 9.8×10^6 cm^{-3} and 6.8 pptv, respectively.

429 As both O_3 and SOA were produced by photochemical reactions during the
430 IMPACT-2 and IMPACT-L campaigns, the SOA/O_3 ratio can be used as an index of OA
431 formation efficiency in a given oxidative condition (Fig. 5) (Herndon et al., 2008; Kondo
432 et al., 2008). The model simulation tends to overestimate maximum SOA
433 concentrations during daytime and underestimate SOA concentrations during nighttime.
434 However, mean SOA concentrations are reproduced by the model to within 25 % of the
435 corresponding observed values (underestimation by 21 % and 13 % during the IMPACT-
436 2 and IMPACT-L campaigns, respectively) (Table 5). In both campaigns, the simulated

437 fitting slopes (with aging processes) are also consistent with observed slopes (and hence,
438 OA formation efficiency): observed and simulated fitting slopes are 0.16 and 0.19 during
439 the IMPACT-2 campaign and 0.15 and 0.20, respectively, during the IMPACT-L
440 campaign.

441 The simulation without aging processes (orange lines and triangles in Fig. 4 and
442 5), which is similar to the simulation using a traditional OA model, severely
443 underestimates mean observed OA concentrations by 76 % and 86 % and fitting slopes
444 by 80 % and 82 % during the IMPACT-2 and IMPACT-L campaigns, respectively. The
445 results show that the emissions of S/IVOCs and the oxidation processes of organic vapors
446 (S/IVOCs and OVOCs) must be considered for reasonable OA simulations in and around
447 Tokyo: including these in the VBS scheme considerably improved the model's ability to
448 simulate OA absolute concentrations and their temporal variations in Tokyo and its
449 outflow area at Kisai.

450 In our simulations, SOA is formed mainly from anthropogenic sources at
451 Komaba and Kisai (77 – 80% of total SOA). The three largest precursors of SOA are
452 aromatics (ARO1 and ARO2, 48%), olefins (OLE1 and OLE2, 13 – 18%), and
453 monoterpenes (TERP, 13 – 16%). OPOA accounts for only 6 – 7% of total SOA at both
454 sites during the simulation periods.

455

456 **4.2. A-FORCE periods (East Asia)**

457 Figures 6a-6d show the time-series of BC and SO_4 at the Fukue and Hedo sites
458 during the A-FORCE campaign (24 March – 26 April 2009). The meteorological
459 conditions during this period are described by Matsui et al. (2013b, 2013c). Synoptic-

460 scale meteorological variations controlled temporal variations of observed aerosol
461 concentrations at Fukue and Hedo: high concentrations during the period covered by a
462 high-pressure system and rapid decreases in concentrations after the passage of a cold
463 front. At Fukue, the site was covered by a high pressure system during the middle of
464 the simulation period (6 – 12 April), and cold fronts passed on 14, 20, and 24 April. The
465 temporal variations of observed BC and SO_4 due to synoptic-scale meteorological
466 variations are generally reproduced by the model simulation. The mean BC
467 concentrations are reproduced well by the model at Fukue and Hedo (normalized mean
468 bias (NMB) of -14% at Fukue and -24% at Hedo). The mean SO_4 concentrations at Fukue
469 are also reproduced well by the model (NMB of -11%, Table 5), while those at Hedo are
470 overestimated by a factor of 2 during the middle and latter parts of the simulation period
471 (NMB of 78%, Table 5).

472 Figures 6e and 6f show the time-series of OA at Fukue and Hedo during the A-
473 FORCE period. At both sites, most of the measured OA was OOA and most of the
474 simulated OA was SOA (shown below). The temporal variations of OA are generally
475 similar to those of SO_4 at both sites. At Fukue, the model overestimates OA
476 concentrations during 7 – 15 April but underestimates them during 28 March – 2 April.
477 The model well reproduces observed OA concentrations during other periods. The
478 period-averaged OA concentrations are slightly overestimated (NMB of 12%, Table 5),
479 but the model simulations agree well with the measurements.

480 At Hedo, simulated OA concentrations are overestimated by 80% (Table 5).
481 The period of OA overestimation corresponds to the period of SO_4 overestimation.
482 Therefore, it is unlikely that the problems in OA formation processes only made the

discrepancy between observed and simulated OA concentrations. The model may overestimate the transport of pollutants, including precursor species and secondary aerosol formation from them. The uncertainties in AMS measurements may also contribute the discrepancy between measurements and model simulations because the observed OA concentrations at Hedo are the lower limit in terms of the collection efficiency (section 3.2).

Observed OOA/OA ratio was estimated to be greater than 95% at Fukue and Hedo (Zhang et al., 2007). Simulated SOA/OA ratio is 84% at Fukue and 83% at Hedo, suggesting that our model simulations tend to underestimate the fraction of SOA to total OA at these measurement sites.

Figures 6g and 6h show the time-series of OA/SO_4 ratio at Fukue and Hedo during the A-FORCE period. The OA/SO_4 ratio is used because both OA and SO_4 at these sites are formed through oxidation processes in the atmosphere. Their oxidation pathways may not be exactly the same (OA is formed from gas-phase oxidation only, but SO_4 is formed from both gas-phase and aqueous-phase oxidation in our model), but as the formation processes of SO_4 are relatively well known compared with those of OA, the OA/SO_4 ratio can be used as an index of OA formation efficiency relative to the amounts of secondary aerosols transported to the measurement sites. The model reproduces reasonably well the period-averaged OA/SO_4 ratio observed at Fukue and Hedo: the observed ratios are 0.89 and 0.58, and the simulated ratios are 0.78 (NMB of -12%) and 0.42 (NMB of -30%), respectively (Table 5).

In contrast, the simulation without aging processes do not capture observed OA mass concentrations and OA/SO_4 ratios. The model without aging processes

506 considerably underestimates both the OA concentrations (by 88% and 83%) and the
507 OA/SO_4 ratio (by 85% and 90%) at Fukue and Hedo, respectively. The results
508 demonstrate that the VBS scheme with aging processes much improves model
509 performance; the scheme realistically simulated OA mass concentrations and their
510 temporal variations and the OA/SO_4 ratio over the outflow regions in East Asia.

511 Simulated SOA is formed mostly from anthropogenic sources at Fukue and Hedo
512 (90 – 91% of total SOA). The three largest sources are aromatics (ARO1 and ARO2,
513 41 – 46%), S/IVOCs (34 – 41%), and monoterpenes (TERP, 7 – 8%). The contributions
514 of OPOA at Fukue and Hedo (34 – 41% of total SOA) are much higher than those at
515 Komaba and Kisai (6 – 7% of total SOA), due to continuous aging processes of organic
516 vapors during transport from source areas to the measurement sites at Fukue and Hedo.

517 The uncertainties in the aging coefficients of S/IVOCs are very large in the VBS
518 scheme. To understand the impact of these uncertainties on simulated OA mass
519 concentrations, we conducted sensitivity simulations with the aging coefficient of 4×10^{-11} cm^3 $molecule^{-1}$ s^{-1} (4 times of the base case, "Aging-4") and 2.5×10^{-12} cm^3 $molecule^{-1}$ s^{-1} (1/4 of the base case, "Aging-0.25") (Fig. 6e and 6f, Table 4). The Aging-4 (Aging-
522 0.25) simulation increased (decreased) period-averaged OA mass concentrations by
523 factors of 3.2 (2.1) and 4.1 (2.4) at Fukue and Hedo, respectively; thus simulated OA
524 concentrations over East Asia are greatly affected by the choice of aging coefficients.
525 Therefore, it is important to improve our understanding of the oxidation processes of
526 organic vapors through laboratory and field measurements and to apply and validate the
527 VBS scheme for various atmospheric conditions.

528

5. Spatial distribution of OA over East Asia

5.1. Impact of aging processes

5.1.1. Mass concentrations and contributions

Next, we examine the spatial distributions of OA over East Asia. In Sect. 5, all particles between 40 nm and 10 μm in diameter were used to calculate OA concentrations. For the simulation with the aging process, POA concentrations at an altitude of about 1 km peak over Southeast Asia and northern and central China (Fig. 7a), corresponding to large source regions of biomass burning and anthropogenic emissions, respectively (Fig. 3a and b). The spatial distribution of OPOA is similar to that of POA (Fig. 7c). ASOA concentrations are high over northern and central China and moderate over southern China, Japan, and Southeast Asia (Fig. 7e). The maximum of BSOA concentration is over Southeast Asia and southern China (Fig. 7g). Total SOA (OPOA + ASOA + BSOA) concentrations are distributed widely over East Asia with peaks over Southeast Asia and northern and central China (Fig. 7i).

The large contribution of BSOA over southern China and Southeast Asia is consistent, at least qualitatively, with previous OA modeling studies (Han et al., 2008; Jiang et al., 2012; Li et al., 2013), in which 65 – 90 % of SOA in southern China was estimated to be biogenic. Several measurement studies have reported mean organic carbon (OC) concentrations in spring over Guangzhou in southern China of 6 – 7 μg m^{-3} (Tao et al., 2012; Huang et al., 2012), over Hong Kong of 6 – 9 μg m^{-3} (Bahadur et al., 2009), and over Bangkok of about 10 μg m^{-3} (Sahu et al., 2011). We compared our simulation results with these measurements, though the meteorological conditions, the amounts of emissions (e.g., biomass burning, biogenic), or both may have differed

552 between those studies and ours. When we assume an OC-to-OA conversion rate of 1.6
553 (Turpin and Lim, 2001), our simulations underestimate observed OA concentrations by
554 35% at Guangzou and by 60 – 70% at Hong Kong and Bangkok. OOA concentrations
555 in the Pearl River Delta region observed with an AMS have also been reported: about 5
556 μg m^{-3} in summer 2006 (Xiao et al., 2011) and in fall 2009 (Li et al., 2013). Our
557 simulations underestimate the observed SOA concentrations by 30 – 40% in this region.
558 The rough comparisons shown above suggest that our OA and SOA simulations over
559 southern China and Southeast Asia are consistent with measurements to within a factor
560 of 3 (underestimation by 30 – 70%). The agreement between measurements and model
561 simulations over southern China and Southeast Asia was much improved by considering
562 aging processes of organic vapors in the VBS scheme.

563 SOA concentrations in the Aging-off simulation are much lower than those in
564 the Aging-on simulation (Fig. 7). By considering aging processes, ASOA, BSOA,
565 OPOA, total SOA, and total OA concentrations over the outer domain increased between
566 440% and 1380% (Fig. 8a and Table 6), demonstrating the importance of aging processes
567 in OA simulations for East Asia. POA concentrations, however, vary less: the Aging-on
568 POA concentrations over the outer domain are about 30% more than those for the Aging-
569 off simulations (Fig. 8a and Table 6). The lower POA concentrations in the Aging-off
570 simulation are likely due to the smaller amounts of low-volatile organic vapors, which
571 are produced by OH oxidation in the Aging-on simulation, and the resulting reduction of
572 OA concentrations in the particulate phase because of the shift of gas-particle partitioning
573 to the gas-phase.

574 In addition to differences in the absolute mass concentrations, the contributions

575 from individual chemical compositions to total OA also differ greatly between the Aging-
576 on and Aging-off simulations (Fig. 8b and c). In the Aging-on simulation, POA, OPOA,
577 ASOA, and BSOA account for 18%, 29%, 26%, and 27% of OA, respectively, over the
578 outer domain. The main precursors of ASOA are aromatics (ARO1 and ARO2, 80% of
579 ASOA), and those of BSOA are monoterpenes (TERP, 55% of BSOA). In the aging-off
580 simulation, POA is dominant (70% of total OA) because of the formation of much less
581 ASOA and BSOA and no OPOA.
582
583 **5.1.2. Sensitivity of aging parameters over East Asia**
584 Table 6 shows the results of the Aging-4 and Aging-0.25 simulations. Similar
585 to the results at Fukue and Hedo (Sect. 4.2), SOA concentrations are highly sensitive to
586 aging coefficients over the simulation domain. The period-averaged mass
587 concentrations of OPOA, ASOA, and BSOA were enhanced (reduced) by factors of 3.3
588 (6.6), 2.0 (3.1), and 1.9 (2.6), respectively, in the Aging-4 (Aging-0.25) simulation over
589 the whole East Asian region (Table 6a). In contrast, POA concentrations are not so
590 sensitive to the aging coefficients. The average POA concentrations were increased by
591 17% in the Aging-4 simulation and decreased by 26% in the Aging-0.25 simulation, both
592 relative to the Aging-on (base) simulation.
593 Increasing the rate constant by a factor of 4 enhances OPOA concentrations
594 (increase by a factor of 3.3) more relative to ASOA (increase by a factor of 2). IVOCs
595 and their aging processes may contribute to the difference in enhancement between
596 OPOA and ASOA because both primary and oxygenated S/IVOCs concentrations in high
597 volatility (C* of 10^6 – 10^2 μg m^{-3}) are lower in the Aging-4 simulation relative to the

598 Aging-on simulation (not shown).

599 OPOA increase from the Aging-on to the Aging-4 simulation is mostly due to
600 faster aging processes of primary and secondary S/IVOCs. ASOA (BSOA) increase
601 from the Aging-on to the Aging-4 simulation is due to faster aging processes of both
602 anthropogenic OVOCs (biogenic OVOCs) and S/IVOCs. The contribution of S/IVOCs
603 aging processes to ASOA and BSOA increases is about one-third of total increases in
604 ASOA and BSOA concentrations from the Aging-on to the Aging-4 simulation (not
605 shown).

606

607 **5.1.3. Interaction of anthropogenic and biogenic sources**

608 The sensitivity simulations shown in Sect. 5.1.3 and 5.2 are summarized in Fig.
609 9. The simulation results with aging processes from biogenic sources only (no aging
610 treatment for S/IVOCs and anthropogenic OVOCs) are shown in Fig. 8a and Table 6 (the
611 Aging-bio simulation in Table 4). The contribution of aging processes from
612 anthropogenic sources (AN-aging) can be estimated from the difference in OA
613 concentrations between the Aging-on (base case) and Aging-bio simulations (Fig. 9).
614 As expected, the impact of AN-aging on OPOA and ASOA over the outer domain is very
615 large: AN-aging enhances OPOA concentrations from 0.0 to 0.37 μg m^{-3} and ASOA
616 concentrations from 0.038 to 0.33 μg m^{-3} (+780%) (Table 6). AN-aging also enhances
617 POA concentrations moderately (+20%, Table 6).

618 BSOA concentrations are also enhanced considerably (+45%) by AN-aging
619 (Table 6). This is because AN-aging produces large amounts of low-volatile organic
620 vapors and OA from anthropogenic VOCs and S/IVOCs, and these vapors shift the gas-

621 particle partitioning ratio of BSOA to the particulate phase. Therefore, AN-aging is very
622 important for OA formation from both anthropogenic and biogenic sources.

623 These results show that BSOA concentrations are substantially enhanced by OA
624 models that can represent realistic OA concentrations from anthropogenic OA in the
625 atmosphere (the VBS scheme in case of this study), even if we do not change the treatment
626 of BSOA formation processes in the model. In this study, the importance of this effect
627 was shown for springtime over East Asia, where anthropogenic and biogenic emissions
628 interact closely. Similar interaction is expected over other large emission sources such
629 as the United States and Europe, implying the importance of AN-aging to BSOA
630 concentrations on hemispherical and global scales. Therefore, to obtain more accurate
631 simulations of BSOA, which is considered to be dominant globally, it is important to use
632 a realistic OA formation scheme for anthropogenic sources.

633 Figure 8a also shows the simulation results with aging processes from
634 anthropogenic sources only (the Aging-an simulation in Table 4). We can estimate the
635 contribution of aging processes from biogenic sources (BIO-aging) by the difference in
636 OA between the Aging-on (base case) and Aging-an simulations (Fig. 9). BIO-aging
637 slightly influences (less than 4 – 7%) POA, OPOA, and ASOA, whereas it is important
638 for BSOA (increased by 210%). Therefore, the enhancement of anthropogenic OA by
639 aging processes of biogenic VOCs is limited. The difference in the importance of AN-
640 aging and BIO-aging is because anthropogenic sources are dominant over East Asia (Fig.
641 8b).

642

643 **5.2. Estimation of controllable OA**

644 We estimate the contribution of OA influenced by anthropogenic emission
645 sources (i.e., controllable OA). Here, we assume that biomass burning emissions are
646 not anthropogenic (not controllable) sources, following the treatment in Carlton et al.
647 (2010). For estimating the contribution of controllable OA over East Asia, we
648 conducted sensitivity simulations with various amounts of anthropogenic emissions
649 ranging from 0% to 200% of base case emissions for both gaseous (CO, NO_x, SO_2, VOCs,
650 and primary S/IVOCs) and aerosol species (POA and BC). Other settings are similar to
651 the base case simulation. Biomass burning, biogenic, and volcanic emissions are not
652 changed in these sensitivity simulations.

653 Period-averaged POA, OPOA, and ASOA concentrations normalized by those
654 in the base case simulation increase almost linearly with anthropogenic emissions over
655 the outer domain in the sensitivity simulations, except for the range of anthropogenic
656 emissions from 0 to 50%, where the contribution from biomass burning sources
657 dominates (Fig. 10). In the simulation without anthropogenic emissions, POA, OPOA,
658 and ASOA decrease to 20%, 9%, and 2%, respectively, of the base case simulation. This
659 is because the reduction of anthropogenic VOCs, NO_x, and POA leads to OA reduction
660 by changing both VOC concentrations and their oxidation rates, and gas-particle
661 partitioning of organic compounds. Controllable OA concentrations can be estimated
662 from the differences in OA between the simulations with (100%) and without (0%)
663 anthropogenic emissions (Fig. 9). The fractions of controllable POA, OPOA, and
664 ASOA are 80%, 91%, and 98%, respectively, in our simulations over all of East Asia.

665 The fractions of POA, OPOA, and ASOA in the simulation without
666 anthropogenic emissions (20%, 9%, and 2% of the base case) are smaller than the

667 fractions expected from emissions, because biomass burning sources account for 30% of
668 POA emissions and 10% of aromatics emissions over the outer domain (Fig. 3c and 3d).
669 An important reason for these smaller fractions is the lower OH concentrations (by a
670 factor of 3) and resulting slower rates of oxidation of organic vapors in the simulation
671 without anthropogenic emissions compared with the base case simulation. In fact, the
672 fraction of low-volatile organics (sum of vapors and aerosols) is smaller in the simulation
673 without anthropogenic emissions (not shown).

674 BSOA mass concentrations are positively related to the amounts of
675 anthropogenic emissions, though the relationship is weaker than POA, OPOA, and ASOA
676 (green line in Fig. 10). The fraction of controllable BSOA is 78% in our estimation;
677 thus a large portion of BSOA is formed through the influence of anthropogenic sources
678 (the enhancement of anthropogenic VOCs, NO_x, and preexisting OA) over East Asia.

679 The period-averaged controllable OA concentrations over the outer domain are
680 1.12 $\mu g\ m^{-3}$ and are higher than the sum of POA, OPOA, and ASOA concentrations (0.94
681 $\mu g\ m^{-3}$). The fraction of controllable OA is 87% (Fig. 11a), suggesting that most of OA
682 is controllable and form anthropogenically in springtime over all of East Asia. The
683 fraction of controllable OA is more than 90% over most of India and China and its outflow
684 regions and 60 – 80% even over Southeast Asia, where BSOA concentrations are high
685 (Fig. 11c), though S/IVOCs emissions and their aging processes have large uncertainties
686 currently (section 2.3). The fraction of controllable $PM_{2.5}$ is 92% in our estimation,
687 though dust and sea salt from natural sources are not considered in this study.

688 We conducted an additional sensitivity simulation to quantify the importance of
689 the oxidant change (OH concentrations by a factor of 3) in the estimation of controllable

690 OA concentrations. In this sensitivity simulation, we excluded emissions from
691 combustion sources for aerosol species and SOA precursors (primary S/IVOCs, aromatics
692 (ARO1 and ARO2), alkanes (ALK4 and ALK5), and olefins (OLE1 and OLE2)) without
693 changing emissions for other gaseous species (CO, NO_x, SO_2, and other VOCs). Period-
694 averaged OH concentrations in this sensitivity simulation were about the same as those
695 in the base case simulation (the difference between two simulations is 7% for OH and
696 0.3% for HO_2 over East Asia). This sensitivity simulation reduced OA concentrations
697 by 73% and BSOA concentrations by 42% over East Asia. These results suggest that
698 the OH change by NO_x and VOCs has a large potential to increase controllable OA
699 amounts over East Asia (from 73% to 87% for total OA and from 42% to 78% for BSOA).
700 Carlton et al. (2010) estimated that more than 50% of BSOA in the eastern United
701 States was controllable. Global modeling studies showed that only 31% (Tsigaridis et
702 al., 2006) and 21% (Hoyle et al., 2009) of the simulated SOA increase from the pre-
703 industrial period to the present was formed directly from anthropogenic VOC, and that
704 the vast majority of the remainder was BSOA enhanced by anthropogenic sources (Hoyle
705 et al., 2011). Spracklen et al. (2011) made top-down estimates of a global SOA budget
706 using both AMS measurements and global model simulations: these estimates suggested
707 that 71% of SOA formed in the atmosphere was controllable. The contribution of
708 controllable OA estimated in this study is higher than these previous estimates. The
709 higher contribution of controllable OA in this study is because anthropogenic sources are
710 dominant over East Asia and OA is enhanced considerably by aging processes of organic
711 vapors from anthropogenic sources (Sect. 5.1.3).
712 Carlton and Turpin (2013) suggested aerosol water produced in anthropogenic

713 aerosols (e.g., SO_4) would enhance biogenic SOA mass concentrations in the eastern U.
714 S. through aqueous-phase chemistry. This process is not considered in our model but
715 could be a potentially important mechanism to enhance controllable OA amounts further
716 in East Asia because SO_4 and OA generally have similar spatial distribution over East
717 Asia.

718 Our estimation of the controllable OA fraction may have large uncertainties
719 because biomass burning emissions are still highly uncertain over East Asia (Matsui et
720 al., 2013a). The estimation may also be highly sensitive to the simulation periods
721 because of large seasonal and interannual variations of biomass burning emissions over
722 East Asia (Matsui et al., 2013a). Since biomass burning emissions are highest during
723 February-April over Southeast Asia and during March-May over China (Matsui et al.,
724 2013a), higher fraction of controllable OA is expected in other seasons in terms of
725 biomass burning emissions.

726 Without aging processes, the domain- and period averaged controllable OA is
727 0.18 $\mu g\ m^{-3}$, and the fraction of controllable OA is 75% (Fig. 11b). The fraction is lower
728 than that in the base case simulation with aging processes. This is because the fraction
729 of OPOA and ASOA, which are mostly formed from anthropogenic sources, is larger in
730 the base case simulation. Both the amounts (from 0.18 to 1.12 $\mu g\ m^{-3}$) and the fraction
731 (from 75% to 87%) of controllable OA are increased by aging processes of organic vapors
732 over East Asia.

733

734 **6. Summary and conclusions**

735 We simulated OA concentrations over East Asia and its outflow region by using

736 the VBS approach. Model simulations were evaluated via comparisons with AMS
737 measurements in and around Tokyo (at the Komaba and Kisai sites during the IMPACT-
738 2 campaign in summer 2003 and the IMPACT-L campaign in summer 2004) and over the
739 outflow region in East Asia (at the Fukue and Hedo sites during the A-FORCE campaign
740 in spring 2009).

741 Model simulations with aging processes of organic vapors (S/IVOCs and
742 OVOCs) reasonably well reproduced mass concentrations, temporal variations, and
743 formation efficiency (i.e., SOA/O_3 and OA/SO_4 ratio) of observed OA: the model
744 reproduced SOA concentrations to within 25% during the IMPACT campaign (NMB of -
745 21% and -13% at Komaba and Kisai, respectively), the SOA/O_3 ratio to within 25% at
746 Komaba and Kisai, OA concentrations to within 15% at Fukue and to within a factor of 2
747 at Hedo, and the OA/SO_4 ratio to within 30% at Fukue and Hedo. In contrast, the
748 simulations without the aging processes did not capture these features. The model
749 without the aging processes severely underestimated mass concentrations (by 76 – 88%)
750 and formation efficiencies of OA (by 80 – 90%) at the 4 measurement sites. The
751 oxidation of organic vapors is therefore essential for realistic OA simulations over East
752 Asia.

753 Concentrations of simulated POA and total SOA (OPOA + ASOA + BSOA)
754 peaked over northern and central China and Southeast Asia, corresponding to large source
755 regions of anthropogenic and biomass burning emissions. Concentrations of ASOA
756 (BSOA) were high over central and northern China (Southeast Asia and southern China).
757 Simulated OA concentrations at an altitude of 1 km over all of East Asia were highly
758 sensitive to aging processes of organic vapors: relative to the results of simulations

759 without aging, total OA concentrations increased from 0.24 to 1.28 μg m^{-3} (+440%).
760 Aging processes also changed OA chemical composition: in the simulation with the aging
761 processes, the contributions of OPOA and ASOA were 29% and 26%, respectively, of
762 total OA, whereas in the simulation without the aging processes, about 70% of total OA
763 was POA.

764 We also examined the importance of the aging processes of organic vapors from
765 anthropogenic (AN-aging) and biogenic sources (BIO-aging). AN-aging was very
766 important for the enhancement of OA formation from both anthropogenic and biogenic
767 sources. AN-aging enhanced BSOA concentrations considerably (+45%), while the
768 enhancement of OPOA and ASOA (SOA from anthropogenic sources) by BIO-aging was
769 very limited (less than 4 – 7%). The difference in the importance of AN-aging and BIO-
770 aging is because anthropogenic sources are dominant over East Asia. These results
771 show that BSOA concentrations are substantially enhanced by OA models that can
772 simulate realistic OA concentrations from anthropogenic sources in the atmosphere, even
773 if we do not change the treatment of BSOA formation processes in the model. Therefore,
774 to obtain more accurate simulations of BSOA, which is considered to be dominant
775 globally, it is important to use a realistic OA formation scheme for anthropogenic sources.

776 The fraction of controllable OA estimated in our simulations was 87%,
777 suggesting that most OA was controllable and formed anthropogenically in springtime
778 over all of East Asia. The fractions of controllable POA, OPOA, ASOA, and BSOA
779 were 80%, 91%, 98%, and 78%, respectively, showing that even a large portion of BSOA
780 was formed through the influence of anthropogenic sources (the enhancement of
781 anthropogenic VOCs, NO_x, and preexisting OA). These fractions were higher than the

782 fraction of anthropogenic emissions (70% of OA emissions and 90% of aromatics
783 emissions over East Asia during the simulation periods). An important reason for these
784 higher controllable fractions was higher OH concentration resulting in faster oxidation
785 rates of organic vapors by considering anthropogenic sources. Both the amounts (from
786 0.18 to 1.12 μg m^{-3}) and the fraction (from 75% to 87%) of controllable OA were
787 increased by including aging processes of organic vapors over East Asia.

788 This study is a first step to examine OA concentrations and their spatial
789 distributions and the anthropogenic-biogenic interaction in OA formation over all of East
790 and Southeast Asia and its outflow regions. Further validations of OA, precursor VOCs,
791 and oxidant species especially over southern China and Southeast Asia, where the
792 contribution of biogenic sources are high, are necessary to understand the behavior of OA
793 and the anthropogenic-biogenic interaction over the Asian region more quantitatively.
794

Acknowledgments.

This work was supported by the Ministry of Education, Culture, Sports, Science, and Technology and the Japan Society for the Promotion of Science (MEXT/JSPS) KAKENHI grant numbers 26740014 and 23221001. This work was also supported by the strategic international cooperative program of the Japan Science and Technology Agency, by the global environment research fund of the Ministry of the Environment, Japan (2A-1101), and by the Alliance for Global Sustainability project of the University of Tokyo. J. D. Fast was supported by the U.S. Department of Energy (DOE) Atmospheric System Research (ASR) program under Contract DE-AC06-76RLO 1830 at PNNL. PNNL is operated for the U.S. DOE by Battelle Memorial Institute. The authors thank Nobuyuki Takegawa at the Research Center for Advanced Science and Technology, University of Tokyo for providing the AMS observation data at the Komaba and Kisai sites during the IMPACT campaign. For a part of the simulations, we used the supercomputer systems in the University of Tokyo and Japan Agency for Marine-Earth Science and Technology.

812 **References**

813 Adhikary, B., Carmichael, G. R, Kulkarni, S., Wei, C., Tang, Y., D'Allura, A., Mena-
814 Carrasco, M., Streets, D. G., Zhang, Q., Pierce, R. B, Al-Saadi, J. A., Emmons, L.
815 K., Pfister, G. G., Avery, M. A., Barrick, J. D., Blake, D. R., Brune, W. H., Cohen,
816 R. C., Dibb, J. E., Fried, A., Heikes, B. G., Huey, L. G., O'Sullivan, D. W., Sachse,
817 G. W., Shetter, R. E., Singh, H. B., Campos, T. L., Cantrell, C. A., Flocke, F. M.,
818 Dunlea, E. J., Jimenez, J. L., Weinheimer, A. J., Crounse, J. D., Wennberg, P. O.,
819 Schauer, J. J., Stone, E. A., Jaffe, D. A., and Reidmiller, D. R.: A regional scale
820 modeling analysis of aerosol and trace gas distributions over the eastern Pacific
821 during the INTEX-B field campaign, Atmos. Chem. Phys., 10, 2091 – 2115, 2010.
822 Ahmadov, R., McKeen, S. A., Robinson, A. L., Bahreini, R., Middlebrook, A. M., de
823 Gouw, J. A., Meagher, J., Hsie, E.-Y., Edgerton, E., Shaw, S., and Trainer, M.: A
824 volatility basis set model for summertime secondary organic aerosols over the
825 eastern United States in 2006, J. Geophys. Res., 117, D06301,
826 doi:10.1029/2011JD016831, 2012.
827 Athanasopoulou, E., Vogel, H., Vogel, B., Tsimpidi, A. P., Pandis, S. N., Knote, C., and
828 Fountoukis, C.: Modeling the meteorological and chemical effects of secondary
829 organic aerosols during an EUCAARI campaign, Atmos. Chem. Phys., 13, 625 –
830 645, 2013.
831 Andersson-Sköld, Y. and Simpson, D.: Secondary organic aerosol formation in northern
832 Europe: A model study, J. Geophys. Res., 106, 7357– 7374,
833 doi:10.1029/2000JD900656, 2001.
834 Bahadur, R., Habib, G., and Russell, L. M.: Climatology of PM2.5 organic carbon

concentrations from a review of ground-based atmospheric measurements by evolved gas analysis, Atmos. Environ., 43, 1591 – 1602, 2009.

Binkowski, F. S. and Shankar, U.: The regional particulate matte model: 1. Model description and preliminary results, J. Geophys. Res., 100(D12), 26191 – 26209, 1995.

Bond, T. C., Doherty, S. J., Fahey, D. W., Forster, P. M., Berntsen, T., DeAngelo, B. J., Flanner, M. G., Ghan, S., Kärcher, B., Koch, D., Kinne, S., Kondo, Y., Quinn, P. K., Sarofim, M. C., Schultz, M. G., Schulz, M., Venkataraman, C., Zhang, H., Zhang, S., Bellouin, N., Guttikunda, S. K., Hopke, P. K., Jacobson, M. Z., Kaiser, J. W., Klimont, Z., Lohmann, U., Schwarz, J. P., Shindell, D., Storelvmo, T., Warren, S. G., and Zender, C. S.: Bounding the role of black carbon in the climate system: A scientific assessment, J. Geophys. Res. Atmos., 118, 5380 – 5552, doi:10.1002/jgrd.50171, 2013.

Carlton, A. G., Pinder, R. W., Bhave, P. V., and Pouliot, G. A.: To what extent can biogenic SOA be controlled?, Environ. Sci. Technol., 44, 3376 – 3380, 2010.

Carlton, A. G. and Turpin, B. J.: Particle partitioning potential of organic compounds is highest in the Eastern US and driven by anthropogenic water, Atmos. Chem. Phys., 13, 10203 – 10214, 2013.

Carmichael, G. R., Tang, Y., Kurata, G., Uno, I., Streets, D., Woo, J.-H., Huang, H., Yienger, J., Lefer, B., Shetter, R., Blake, D., Atlas, E., Fried, A., Apel, E., Eisele, F., Cantrell, C., Avery, M., Barrick, J., Sachse, G., Brune, W., Sandholm, S., Kondo, Y., Singh, H., Talbot, R., Bandy., A., Thorton, D., Clarke, A., and Heikes, B.: Regional-scale chemical transport modeling in support of the analysis of

858 observations obtained during the TRACE-P experiment, J. Geophys. Res.,
859 108(D21), 8823, doi:10.1029/2002JD003117, 2003.
860 Carter, W. P. L.: Documentation of the SAPRC-99 Chemical Mechanism for VOC
861 Reactivity Assessment, Report to the California Air Resources Board. College of
862 Engineering, Center for Environmental Research and Technology, University of
863 California at Riverside, CA. Contracts 92–329 and 95–308, available at:
864 http://www.cert.ucr.edu/~carter/reactdat.htm, 2000.
865 Chung, S. and Seinfeld, J. H.: Global distribution and climate forcing of carbonaceous
866 aerosols, J. Geophys. Res., 107(D19), 4407, doi:10.1029/2001JD001397, 2002.
867 de Gouw, J. and Jimenez, J. L.: Organic aerosols in the Earth's atmosphere, Environ. Sci.
868 Technol., 43, 7614 – 7618, 2009.
869 Dentener, F., Kinne, S., Bond., T., Boucher, O., Cofala, J., Generoso, S., Ginoux, P.,
870 Gong, S., Hoelzemann, J. J., Ito, A., Marelli, L., Penner, J. E., Putaud, J.-P., Textor,
871 C., Schulz, M., van der Werf, G. R., and Wilson, J.: Emissions of primary aerosol
872 and precursor gases in the years 2000 and 1750 prescribed data-sets for AeroCom,
873 Atmos. Chem. Phys., 6, 4321 – 4344, 2006.
874 Donahue, N. M., Robinson, A. L., Stanier, C. O., and Pandis, S. N.: Coupled partitioning,
875 dilution, and chemical aging of semivolatile organics, Environ. Sci. Technol., 40,
876 2635 – 2643, 2006.
877 Donahue, N. M., Epstein, S. A., Pandis, S. N., and Robinson, A. L.: A two-dimensional
878 volatility basis set: 1. Organic-aerosol mixing thermodynamics, Atmos. Chem.
879 Phys., 11, 3303 – 3318, 2011.
880 Easter, R. C., Ghan, S. J., Zhang, Y., Saylor, R. D., Chapman, E. G., Laulainen, N. S.,

881 Abdul-Razzak, H., Leung, L. R., Bian, X. and Zaveri, R. A.: MIRAGE: Model
882 description and evaluation of aerosols and trace gases, J. Geophys. Res., 109,
883 D20210, doi:10.1029/2004JD004571, 2004.
884 Ervens, B., Turpin, B. J., and Weber, R. J.: Secondary organic aerosol formation in cloud
885 droplets and aqueous particles (aqSOA): a review of laboratory, field and model
886 studies, Atmos. Chem. Phys., 11, 11069 – 11102, 2011.
887 Fahey, K. M. and Pandis, S. N.: Optimizing model performance: Variable size resolution
888 in cloud chemistry modeling, Atmos. Environ., 35, 4471– 4478, 2001.
889 Farina, S. C., Adams, P. J., and Pandis, S. N.: Modeling global secondary organic aerosol
890 formation and processing with the volatility basis set: Implications for
891 anthropogenic secondary organic aerosol, J. Geophys. Res., 115, D09202,
892 doi:10.1029/2009JD013046, 2010.
893 Fast, J. D., Gustafson Jr., W. I., Easter, R. C., Zaveri, R. A., Barnard, J. C., Chapman, E.
894 G., Grell, G. A., and Peckham, S. E.: Evolution of ozone, particulates, and aerosol
895 direct radiative forcing in the vicinity of Houston using a fully coupled
896 meteorology-chemistry-aerosol model, J. Geophys. Res., 111, D21305,
897 doi:10.1029/2005JD006721, 2006.
898 Fountoukis, C., Racherla, P. N., Denier van der Gon, H. A. C., Polymeneas, P.,
899 Charalampidis, P. E., Pilinis, C., Wiedensohler, A., Dall'Osto, M., O'Dowd, C., and
900 Pandis, S. N.: Evaluation of a three-dimensional chemical transport model
901 (PMCAMx) in the European domain during the EUCAARI May 2008 campaign,
902 Atmos. Chem. Phys., 11, 10331 – 10347, 2011.
903 George, I. J., Vlasenko, A., Slowik, J. G., Broekhuizen, K., and Abbatt, J. P. D.:

904 Heterogeneous oxidation of saturated organic aerosols by hydroxyl radicals: Uptake
905 kinetics, condensed-phase products, and particle size change, Atmos. Chem. Phys.,
906 7, 4187 – 4201, 2007.
907 George, I. J., Slowik, J., and Abbatt, J. P. D.: Chemical aging of ambient organic aerosol
908 from heterogeneous reaction with hydroxyl radicals, Geophys. Res. Lett., 35,
909 L13811, doi:10.1029/2008GL033884, 2008.
910 Goldstein, A. H. and Galbally, I. E.: Known and unexplored organic constituents in the
911 Earth's atmosphere, Environ. Sci. Technol., 41, 1514 – 1521, 2007.
912 Grell, G. A., Peckham, S. E., Schmitz, R., McKeen, S. A., Frost, G., Skamarock, W. C.,
913 and Eder, B: Fully coupled ''online'' chemistry within the WRF model, Atmos.
914 Environ., 39, 6957 – 6975, 2005.
915 Guenther, A., Karl, T., Harley, P., Wiedinmyer, C., Palmer, P. I., and Geron, C.: Estimates
916 of global terrestrial isoprene emissions using MEGAN (Model of Emissions of
917 Gases and Aerosols from Nature), Atmos. Chem. Phys., 6, 3181 – 3210, 2006.
918 Hallquist, M., Wenger, J. C., Baltensperger, U., Rudich, Y., Simpson, D., Claeys, M.,
919 Dommen, J., Donahue, N. M., George, C., Goldstein, A. H., Hamilton, J. F.,
920 Herrmann, H., Hoffmann, T., Iinuma, Y., Jang, M., Jenkin, M. E., Jimenez, J. L.,
921 Kiendler-Scharr, A., Maenhaut, W., McFiggans, G., Mental, F., Monod, A., Převôt,
922 A. S. H., Seinfeld, J. H., Surratt, J. D., Szmigielski, R., and Wildt, J.: The formation,
923 properties and impact of secondary organic aerosol: current and emerging issues,
924 Atmos. Chem. Phys., 9, 5155 – 5236, 2009.
925 Han, Z., Zhang, R., Wang, Q., Wang, W., Cao, J., and Xu, J.: Regional modeling of
926 organic aerosols over China in summertime, J. Geophys. Res., 113, D11202,

927 doi:10.1029/2007JD009436, 2008.
928 Heald, C. L., Jacob, D. J., Park, R. J., Russell, L. M., Huebert, B. J., Seinfeld, J. H., Liao,
929 H., and Weber, R. J.: A large organic aerosol source in the free troposphere missing
930 from current models, Geophys. Res. Lett., 32, L18809, doi:10.1029/2005GL023831,
931 2005.
932 Heald, C. L., Henze, D. K., Horowitz, L. W., Feddema, J., Lamarque, J.-F., Guenther, A.,
933 Hess, P. G., Vitt, F., Seinfeld, J. H., Goldstein, A. H., and Fung, I.: Predicted change
934 in global secondary organic aerosol concentrations in response to future climate,
935 emissions, and land use change, J. Geophys. Res., 113, D05211,
936 doi:10.1029/2007JD009092, 2008.
937 Heald, C. L., Ridley, D. A., Kreidenweis, S. M., and Drury, E. E.: Satellite observations
938 cap the atmospheric organic aerosol budget, Geophys. Res. Lett., 37, L24808,
939 doi:10.1029/2010GL045095, 2010.
940 Heald, C. L., Coe, H., Jimenez, J. L., Weber, R. J., Bahreini, R., Middlebrook, A. M.,
941 Russell, L. M., Jolleys, M., Fu, T.-M., Allan, J. D., Bower, K. N., Capes, G., Crosier,
942 J., Morgan, W. T., Robinson, N. H., Williams, P. I., Cubison, M. J., DeCarlo, P. F.,
943 and Dunlea, E. J.: Exploring the vertical profile of atmospheric organic aerosol:
944 comparing 17 aircraft field campaigns with a global model, Atmos. Chem. Phys.,
945 11, 12673 – 12696, 2011.
946 Herndon, S. C., Onasch, T. B., Wood, E. C., Kroll, J. H., Canagaratna, M. R., Jayne, J.
947 T., Zavala, M. A., Knighton, W. B., Mazzoleni, C., Dubey, M. K., Ulbrich, I. M.,
948 Jimenez, J. L., Seila, R., de Gouw, J. A., de Foy, B., Fast, J., Molina, L. T., Kolb,
949 C. E., and Worsnop, D. R.: Correlation of secondary organic aerosol with odd

oxygen in Mexico City, Geophys. Res. Lett., 35, L15804, doi:10.1029/2008GL034058, 2008.

Hodzic, A., Jimenez, J. L., Madronich, S., Canagaratna, M. R., DeCarlo, P. F., Kleinman, L., and Fast, J.: Modeling organic aerosols in a megacity: potential contribution of semi-volatile and intermediate volatility primary organic compounds to secondary organic aerosol formation, Atmos. Chem. Phys., 10, 5491 – 5514, 2010.

Hoyle, C. R., Myhre, G., Berntsen, T. K., and Isaksen, I. S. A.: Anthropogenic influence on SOA and the resulting radiative forcing, Atmos. Chem. Phys., 9, 2715 – 2728, 2009.

Hoyle, C. R., Boy. M., Donahue, N. M., Fry, J. L., Glasius, M., Guenther, A., Hallar, A. G., Huff Hartz, K., Petter, M. D., Petäjä, T., Rosenoern, T., and Sullivan, A. P.: A review of the anthropogenic influence on biogenic secondary organic aerosol, Atmos. Phys. Chem., 11, 321 – 343, 2011.

Huang, H., Ho, K. F., Lee, S. C., Tsang, P. K., Ho, S. S. H., Zou, C. W., Zou, S. C., Cao, J. J., and Xu, H. M.: Characteristics of carbonaceous aerosol in $PM_{2.5}$: Pearl Delta River Region, China, Atmos. Res., 104-105, 227 – 236, 2012.

Iinuma, Y., Böge, O., Gnauk, T. and Herrmann, H.: Aerosol-chamber study of the α-pinene/O_3 reaction: Influence of particle acidity on aerosol yields and products, Atmos. Environ., 38, 761 – 773, 2004.

Jacobson, M. Z., Turco, R. P., Jensen, E. J., and Toon, O. B.: Modeling coagulation among particles of different composition and size, Atmos. Environ., 28, 1327–1338, 1994.

Jathar, S. H., Farina, S. C., Robinson, A. L., and Adams, P. J.: The influence off semi-

973 volatile and reactive primary emissions on the abundance and properties of global
974 organic aerosol, Atmos. Chem. Phys., 11, 7727 – 7746, 2011.
975 Jiang, F., Liu, Q. Huang, X. X., Wang, T. J., Zhuang, B. L., and Xie, M.: Regional
976 modeling of secondary organic aerosol over China using WRF/Chem, J. Aerosol
977 Sci., 43, 57 – 73, 2012.
978 Jimenez, J. L., Canagaratna, M. R., Donahue, N. M., et al.: Evolution of organic aerosols
979 in the atmosphere, Science, 326, 1525 – 1529, 2009.
980 Kalberer, M., Paulsen, D., Sax, M., Steinbacher, M., Dommen, J., Prevot, A. S. H.,
981 Fisseha, R., Weingartner, E., Frankevich, V., Zanobi, R., Baltensperger, U.:
982 Identification of polymers as major components of atmospheric organic aerosols,
983 Science, 303, 1659 – 1662, 2004.
984 Kanakidou, M., Seinfeld, J. H., Pandis, S. N., Barnes, I., Dentener, F. J., Facchini, M. C.,
985 Van Dingenen, R., Ervens, B., Nenes, A., Nielsen, C. J., Swietlicki, E., Putaud, J.
986 P., Balkanski, Y., Fuzzi, S., Horth, J., Moortgat, G. K., Winterhalter, R., Myhre, C,
987 E. L., Tsigaridis, K., Vignati, E., Stephanou, E. G., and Wilson, J.: Organic aerosol
988 and global climate modeling: A review, Atmos. Chem. Phys., 5, 1053– 1123, 2005.
989 Kanaya, Y., Cao, R., Akimoto, H., Fukuda, M., Komazaki, Y., Yokouchi, Y., Koike, M.,
990 Tanimoto, H., Takegawa, N., and Kondo, Y.: Urban photochemistry in central
991 Tokyo: 1. Observed and modeled OH and HO2 radical concentrations during the
992 winter and summer of 2004, J. Geophys. Res., 112, D21312,
993 doi:10.1029/2007JD008670, 2007.
994 Kannari, A., Baba, T., Ueda, H., Tonooka, Y., and Matsuda, K.: Development of a grid
995 database on atmospheric pollutants emissions in Japan, (in Japanese), J. Jpn. Soc.

996 Atmos. Environ., 39(6), 257– 271, 2004.
997 Kondo, Y., Komazaki, Y., Miyazaki, Y., Moteki, N., Takegawa, N., Kodama, D.,
998 Deguchi, S., Nogami, M., Fukuda, M., Miyakawa, T., Morino, Y., Koike, M.,
999 Sakurai, H., and Ehara, K.: Temporal variations of elemental carbon in Tokyo, J.
1000 Geophys. Res., 111, D12205, doi:10.1029/2005JD006257, 2006.
1001 Kondo, Y., Miyazaki, Y., Takegawa, N., Miyakawa, T., Weber, R. J., Jimenez, J. L.,
1002 Zhang, Q., and Worsnop, D. R.: Oxygenated and water-soluble organic aerosols in
1003 Tokyo, J. Geophys. Res., 112, D01203, doi:10.1029/2006JD007056, 2007.
1004 Kondo, Y. Morino, Y., Fukuda, M., Kanaya, Y., Miyazaki, Y., Takegawa, N., Tanimoto,
1005 H., McKenzie, R., Johnston, P., Blake, D. R., Murayama, T., and Koike, M:
1006 Formation and transport of oxidized reactive nitrogen, ozone, and secondary
1007 organic aerosol in Tokyo, J. Geophys. Res., 113, D21310,
1008 doi:10.1029/2008JD010134, 2008.
1009 Kondo, Y., Takegawa, N., Matsui, H., Miyakawa, T., Koike, M., Miyazaki, Y., Kanaya,
1010 Y., Mochida, M., Kuwata, M., Morino, Y., and Shiraiwa, M.: Formation and
1011 transport of aerosols in Tokyo in relation to their physical and chemical properties:
1012 A review, J. Meteor. Soc. Japan, 88, 597 – 624, 2010.
1013 Kondo, Y., Oshima, N., Kajino, M., Mikami, R., Moteki, N., Takegawa, N., Verma, R.
1014 L., Kajii, Y., Kato, S., and Takami, A.: Emissions of black carbon in East Asia
1015 estimated from observations at a remote site in the East China Sea, J. Geophys. Res.,
1016 116, D16201, doi:10.1029/2011JD015637, 2011.
1017 Koo, B., Ansari, A. S., and Pandis, S. N.: Integrated approaches to modeling the organic
1018 and inorganic atmospheric aerosol components, Atmos. Environ., 37, 4757 – 4768,

2003.

Kroll, J. H., Smith, J. D., Che, D. L., Kessler, S. H., Worsnop, D. R., and Wilson, K. R.: Measurement of fragmentation and functionalization pathways in the heterogeneous oxidation of oxidized organic aerosol, Phys. Chem. Chem. Phys. 11, 8005 – 8014, 2009.

Lane, T. E., Donahue, N. M., and Pandis, S. N.: Effect of NOx on secondary organic aerosol concentrations, Environ. Sci. Technol., 42, 6022 – 6027, 2008a.

Lane, T. E., Donahue, N. M., and Pandis, S. N.: Simulating secondary organic aerosol formation using the volatility basis-set approach in a chemical transport model, Atmos. Environ., 42, 7439 – 7451, 2008b.

Levine, S. Z. and Schwartz, S. E.: In-cloud and below-cloud scavenging of nitric acid vapor, Atmos. Environ., 16, 1725 – 1734, 1982.

Li, N., Fu, T.-M., Cao, J., Lee, S., Huang, X.-F., He, L.-Y., Ho, K.-F., Fu, J. S., and Lam, Y.-F.: Sources of secondary organic aerosols in the Pearl River Delta region in fall: Contributions from the aqueous reactive uptake of dicarbonyls, Atmos. Environ., 76, 200 – 207, 2013.

Lim, B., Tan, Y., Perri, M. J., Seitzinger, S. P., and Turpin, B. J.: Aqueous chemistry and its role in secondary organic aerosol (SOA) formation, Atmos. Chem. Phys., 10, 10521 – 10539, 2010.

Liu, J., Horowitz, L. W., Fan, S., Carlton, A. G., and Levy II, H.: Global in-cloud production of secondary organic aerosols: Implementation of a detailed chemical mechanism in the GFDL atmospheric model AM3, J. Geophys. Res., 117, D15303, doi:10.1029/2012JD017838, 2012.

1042 Mahmud, A. and Barsanti, K.: Improving the representation of secondary organic aerosol
1043 (SOA) in the MOZART-4 global chemical transport model, Geosci. Model. Dev.,
1044 6, 961 – 980, 2013.
1045 Matsui, H., Koike, M. Takegawa, N. Kondo, Y., Griffin, R. J., Miyazaki, Y., Yokouchi,
1046 Y., and Ohara, T.: Secondary organic aerosol formation in urban air: Temporal
1047 variations and possible contributions from unidentified hydrocarbons, J. Geophys.
1048 Res., 114, D04201, doi:10.1029/2008JD010164, 2009a.
1049 Matsui, H., Koike, M., Kondo, Y., Takegawa, N., Kita, K., Miyazaki, Y., Hu, M., Chang,
1050 S.-Y., Blake, D. R., Fast, J. D., Zaveri, R. A., Streets, D. G., Zhang, Q., and Zhu, T:
1051 Spatial and temporal variations of aerosols around Beijing in summer 2006: Model
1052 evaluation and source apportionment, J. Geophys. Res., 114, D00G13,
1053 doi:10.1029/2008JD010906, 2009b.
1054 Matsui, H., Koike, M., Kondo, Y., Takegawa, N., Fast, J. D., Pöschl, U., Garland, R. M.,
1055 Andreae, M. O., Wiedensohler, A., Sugimoto, N., and Zhu, T.: Spatial and temporal
1056 variations of aerosols around Beijing in summer 2006: 2. Local and column aerosol
1057 optical properties, J. Geophys. Res., 115, D22207, doi:10.1029/2010JD013895,
1058 2010.
1059 Matsui, H., Kondo, Y., Moteki, N., Takegawa, N., Sahu, L. K., Zhao, Y., Fuelberg, H. E.,
1060 Sessions, W. R., Diskin, G., Blake, D. R., Wisthaler, A., and Koike, M.: Seasonal
1061 variation of the transport of black carbon aerosol from the Asian continent to the
1062 Arctic during the ARCTAS aircraft campaign, J. Geophys. Res., 116, D05202,
1063 doi:10.1029/2010JD015067, 2011a.
1064 Matsui, H., Kondo, Y., Moteki, N., Takegawa, N., Sahu, L. K., Koike, M., Zhao, Y.,

1065 Fuelberg, H. E., Sessions, W. R., Diskin, G., Anderson, B. E., Blake, D. R.,
1066 Wisthaler, A., Cubison, M. J., and Jimenez, J. L.: Accumulation-mode aerosol
1067 number concentrations in the Arctic during the ARCTAS aircraft campaign: Long-
1068 range transport of polluted and clean air from the Asian continent, J. Geophys. Res.,
1069 116, D20217, doi:10.1029/2011JD016189, 2011b.
1070 Matsui, H., Koike, M., Kondo, Y., Takegawa, N., Wiedensohler, A., Fast, J. D., and
1071 Zaveri, R. A.: Impact of new particle formation on the concentrations of aerosols
1072 and cloud condensation nuclei around Beijing, J. Geophys. Res., 116, D19208,
1073 doi:10.1029/2011JD016025, 2011c.
1074 Matsui, H., Koike, M., Kondo, Y., Oshima, N., Moteki, N., Kanaya, Y., Takami, A., and
1075 Irwin, M.: Seasonal variations of Asian black carbon outflow to the Pacific:
1076 Contribution from anthropogenic sources in China and biomass burning sources in
1077 Siberia and Southeast Asia, J. Geophys. Res. Atmos., 118, 9948–9967,
1078 doi:10.1002/jgrd.50702, 2013a.
1079 Matsui, H., Koike, M., Kondo, Y., Moteki, N., Fast, J. D., and Zaveri, R. A.: Development
1080 and validation of a black carbon mixing state resolved three-dimensional model:
1081 Aging processes and radiative impact, J. Geophys. Res. Atmos., 118,
1082 doi:10.1029/2012JD018446, 2013b.
1083 Matsui, H., Koike, M., Takegawa, N., Kondo, Y., Takami, A., Takamura, T., Yoon, S.,
1084 Kim, S.-W., Lim, H.-C., and Fast, J. D.: Spatial and temporal variations of new
1085 particle formation in East Asia using an NPF-explicit WRF-chem model: North-
1086 south contrast in new particle formation frequency, J. Geophys. Res. Atmos., 118,
1087 doi:10.1002/jgrd.50821, 2013c.

McKeen, S., Chung, S. H., Wilczak, J., Grell, G., Djalalova, I., Peckham, S., Gong, W., Bouchet, V., Moffet, R., Tang, Y., Carmichael, G. R., Mathur, R., and Yu, S.: Evaluation of several $PM_{2.5}$ forecast models using data collected during the ICARTT/NEAQS 2004 field study, J. Geophys. Res., 112, D10S20, doi:10.1029/2006JD007608, 2007.

Murphy, B. N., Donahue, N. M., Fountoukis, C., and Pandis S. N.: Simulating the oxygen content of ambient organic aerosol with the 2D volatility basis set, Atmos. Chem. Phys. 11, 7859 – 7873, 2011.

Murphy, B. N., Donahue, N. M., Fountoukis, C., Dall'Osto, N., O'Dowd, C., Kiendler-Scharr, A., and Pandis, S. N.: Functionalization and fragmentation during ambient organic aerosol aging: application of the 2-D volatility basis set to field studies, Atmos., Chem., Phys., 12, 10797 – 10816, 2012.

Odum, J. R., Hoffmann, T., Bowman, F., Collins, D., Flagan, R. C., and Seinfeld, J. H.: Gas/particle partitioning and secondary organic aerosol yields, Environ. Sci. Technol., 30, 2580 – 2585, 1996.

Odum, J. R., Jungkamp, T. P. W., Griffin, R. J., Flagan, R. C., and Seinfeld, J. H.: The atmospheric aerosol-forming potential of whole gasoline vapor, Science, 276, 96 – 99, 1997.

Oshima, N., Kondo, Y., Moteki, N., Takegawa, N., Koike, M., Kita. K., Matsui, H., Kajino, M., Nakamura, H., Jung, J. S., and Kim, Y. J.: Wet removal of black carbon in Asian outflow: Aerosol Radiative Forcing in East Asia (A-FORCE) aircraft campaign, J. Geophys. Res., 117, D03204, doi:10.1029/2011JD016552, 2012.

Oshima., N., Koike, M., Kondo, Y., Nakamura, H., Moteki, N., Matsui, H., Takegawa,

1111 N., and Kita, K.: Vertical transport mechanisms of black carbon over East Asia in
1112 spring during the A-FORCE aircraft campaign, J. Geophys. Res. Atmos., 118,
1113 13175 – 13198, doi:10.1002/2013JD020262, 2013.
1114 Pye, H. O. T. and Seinfeld, J. H.: A global perspective on aerosol from low-volatility
1115 organic compounds, Atmos. Chem. Phys., 10, 4377 – 4401, 2010.
1116 Ramanathan, V., Crutzen, P. J., Kiehl, J. T., and Rosenfeld, D.: Aerosols, climate, and
1117 the hydrological cycle, Science, 294(5549), 2119–2124, 2001.
1118 Robinson, A. L., Donahue, N. M., Shrivastava, M. K., Weitkamp, E. A., Sage, A. M.,
1119 Grieshop, A. P., Lane, T. E., Pierce, J. R., and Pandis, S. N.: Rethinking organic
1120 aerosols: Semivolatile emissions and photochemical aging, Science, 315, 1259 –
1121 1262, 2007.
1122 Sahu, L. K., Kondo, Y., Miyazaki, Y., Pongkiatkul, P., and Kim Oanh, N. T.: Seasonal
1123 and diurnal variations of black carbon and organic carbon aerosols in Bangkok, J.
1124 Geophys. Res., 116, D15302, doi:10.1029/2010JD015563, 2011.
1125 Schell, B., Ackermann, I. J., Hass, H., Binkowski, F. S., and Ebel, A.: Modeling the
1126 formation of secondary organic aerosol within a comprehensive air quality model
1127 system, J. Geophys. Res., 106, 28275–28293, doi:10.1029/2001JD000384, 2001.
1128 Shirai, T., Yokouchi, Y., Blake, D. R., Kita, K., Izumi, K., Koike, M., Komazaki, Y.,
1129 Miyazaki, Y., Fukuda, M., and Kondo, Y.: Seasonal variations of atmospheric C2–
1130 C7 nonmethane hydrocarbons in Tokyo, J. Geophys. Res., 112, D24305,
1131 doi:10.1029/2006JD008163, 2007.
1132 Shrivastava, M., Fast, J., Easter, R., Gustafson Jr., W. I., Zaveri, R. A., Jimenez, J. L.,
1133 Saide, P., and Hodzic, A.: Modeling organic aerosols in a megacity: comparison of

simple and complex representations of the volatility basis set approach, Atmos. Chem. Phys., 11, 6639 – 6662, 2011.

Shrivastava, M., Zelenyuk, A., Imre, D., Easter, R., Beranek, J., Zaveri, R. A., and Fast, J.: Implications of low volatility SOA and gas-phase fragmentation reactions on SOA loadings and their spatial and temporal evolution in the atmosphere, J. Geophys. Res. Atmos., 118, 3328–3342, doi:10.1002/jgrd.50160, 2013.

Skamarock, W. C., Klemp, J. B., Dudhia, J., Gill, D. O., Barker, D. M., Wang, W., and Powers, J. G.: A description of the advanced research WRF version 3, NCAR Tech. Note, NCAR/TN-475+STR, Natl. Cent. Atmos. Res., Boulder, Colo, 2008.

Spracklen, D. V., Jimenez, J. L., Carslaw, K. S., Worsnop, D. R., Evans, M. J., Mann, G. W., Zhang, Q., Canagaratna, M. R., Allan, J., Coe, H., McFiggans, G., Rap, A., and Forster, P.: Aerosol mass spectrometer constraint on the global secondary organic aerosol budget, Atmos. Chem. Phys., 11, 12109 – 12136, 2011.

Streets, D. G., Bond, T. C., Carmichael, G. R., Fernandes, S. D., Fu, Q., He, D., Klimont, Z., Nelson, S. M., Tsai, N. Y., Wang, M. Q., Woo, J.-H., and Yarber, K. F.: An inventory of gaseous and primary aerosol emissions in Asia in the year 2000, J. Geophys. Res., 108(D21), 8809, doi:10.1029/2002JD003093, 2003.

Takami, A., Miyoshi, T., Shimono, A., and Hatakeyama, S.: Chemical composition of fine aerosol measured by AMS at Fukue Island, Japan, during APEX period, Atmos. Environ., 39, 4913–4924, 2005.

Takami, A., Miyoshi, T., Shimono, A., Kaneyasu, N., Kato, S., Kajii, Y., and Hatakeyama, S.: Transport of anthropogenic aerosols from Asia and subsequent chemical transformation, J. Geophys. Res., 112, D22S31, doi:10.1029/2006JD008120, 2007.

1157 Takegawa, N., Miyazaki, Y., Kondo, Y., Komazaki, Y., Miyakawa, T., Jimenez, J. L.,
1158 Jayne, J. T., Worsnop, D. R., Allan, J., and Weber, R. J.: Characterization of an
1159 Aerodyne aerosol mass spectrometer (AMS): Intercomparison with other aerosol
1160 instruments, Aerosol Sci. Technol., 39, 760–770, 2005.
1161 Takegawa, N., T. Miyakawa, Kondo, Y., Blake, D. R., Kanaya, Y., Koike, M., Fukuda,
1162 M., Komazaki, Y., Miyazaki, Y., Shimono, A., and Takeuchi, T.: Evolution of
1163 submicron organic aerosol in polluted air exported from Tokyo, Geophys. Res. Lett.,
1164 33, L15814, doi:10.1029/2006GL025815, 2006a.
1165 Takegawa, N., Miyakawa, T., Kondo, Y., Jimenez, J. L., Zhang, Q., Worsnop, D. R., and
1166 Fukuda, M.: Seasonal and diurnal variations of submicron organic aerosols in
1167 Tokyo observed using the Aerodyne aerosol mass spectrometer, J. Geophys. Res.,
1168 111, D11206, doi:10.1029/2005JD006515, 2006b.
1169 Tao, J., Shen, Z. Zhu, C., Yue, J., Cao, J., Liu, S., Zhu, L., and Zhang, R.: Seasonal
1170 variations and chemical characteristics of sub-micrometer particles (PM_1) in
1171 Guangzhou, China, Atmos. Res., 118, 222 – 231, 2012.
1172 Tsigaridis, K. and Kanakidou, M.: Global modelling of secondary organic aerosol in the
1173 troposphere: a sensitivity analysis, Atmos. Chem. Phys., 3, 1849 – 1869, 2003.
1174 Tsigaridis, K. and Kanakidou, M.: Secondary organic aerosol importance in the future
1175 atmosphere, Atmos. Environ., 41, 4682–4692, 2007.
1176 Tsigaridis, K., Krol, M., Dentener, F. J., Balkanski, Y., Lathiere, J., Metzger, S.,
1177 Hauglustaine, D. A., and Kanakidou, M.: Change in global aerosol composition
1178 since preindustrial times, Atmos. Chem. Phys., 6, 5143 – 5162, 2006.
1179 Tsimpidi, A. P., Karydis, V. A., Zavala, M., Lei, W., Molina, L., Ulbrich, I. M., Jimenez,

J. L., and Pandis, S. N.: Evaluation of the volatility basis-set approach for the simulation of organic aerosol formation in the Mexico City metropolitan area, Atmos. Chem. Phys., 10, 525 – 546, 2010.

Tsimpidi, A. P., Karydis, V. A., Zavala, M., Lei, W., Bei, N., Molina, L., and Pandis S. N.: Sources and production of organic aerosol in Mexico City: insights from the combination of a chemical transport model (PMCAMx-2008) and measurements during MILAGRO, Atmos. Chem. Phys., 11, 5153 – 5168, 2011.

Turpin, B. J. and Lim, H. J.: Species contributions to $PM_{2.5}$ mass concentrations: Revisiting common assumptions for estimating organic mass, Aerosol Sci. Technol., 35, 602– 610, 2001.

Utembe, S. R., Cooke, M. C., Archibald, A. T., Shallcross, D. E., Derwent, R. G., and Jenkin, M. E.: Simulating secondary organic aerosol in a 3-D Lagrangian chemistry transport model using the reduced Common Representative Intermediates mechanism (CRI v2-R5), Atmos. Environ., 45, 1604 – 1614, 2011.

van der Werf, G. R., Randerson, J. T., Giglio, L., Collatz, G. J., Mu, M., Kasibhatla, P. S., Morton, D. C., DeFries, R. S., Jin, Y., and van Leeuwen, T. T.: Global fire emissions and the contribution of deforestation, savanna, forest, agricultural, and peat fires (1997 – 2009), Atmos. Chem. Phys., 10, 11707 – 11735, 2010.

Wesely, M. L.: Parameterization of surface resistances to gaseous dry deposition in regional-scale numerical models, Atmos. Environ, 23, 1293–1304, 1989.

Wexler, A. S., Lurmann, F. W., and Seinfeld, J. H.: Modelling urban and regional aerosols. Part I: Model development, Atmos. Environ., 28, 531–546, 1994.

Xiao, R. Takegawa, N., Zheng, M., Kondo, Y., Miyazaki, Y., Miyakawa, T., Hu, M.,

1203 Shao, M., Zeng, L., Gong, Y., Lu, K., Deng, Z., Zhao, Y., and Zhang, Y. H.:
1204 Characterization and source apportionment of submicron aerosol with aerosol mass
1205 spectrometer during the PRIDE-PRD 2006 campaign, Atmos. Chem. Phys., 11,
1206 6911 – 6929, 2011.
1207 Zaveri, R. A. and Peters, L. K.: A new lumped structure photochemical mechanism for
1208 large-scale applications, J. Geophys. Res., 104, 30,387– 30,415,
1209 doi:10.1029/1999JD900876, 1999.
1210 Zaveri, R. A., Easter, R. C., and Wexler, A. S.: A new method for multicomponent
1211 activity coefficients of electrolytes in aqueous atmospheric aerosols, J. Geophys.
1212 Res., 110, D02201, doi:10.1029/2004JD004681, 2005a.
1213 Zaveri, R. A., Easter, R. C., and Peters, L. K.: A computationally efficient
1214 Multicomponent Equilibrium Solver for Aerosols (MESA), J. Geophys. Res., 110,
1215 D24203, doi:10.1029/2004JD005618, 2005b.
1216 Zaveri, R. A., Easter, R. C., Fast, J. D., and Peters, L. K.: Model for Simulating Aerosol
1217 Interactions and Chemistry (MOSAIC), J. Geophys. Res., 113, D13204,
1218 doi:10.1029/2007JD008782, 2008.
1219 Zhang, Q., Alfarra, M. R., Worsnop, D. R., Allan, J. D., Coe, H., Canagaratna, M. R., and
1220 Jimenez, J. L.: Deconvolution and quantification of hydrocarbon-like and
1221 oxygenated organic aerosols based on aerosol mass spectrometry, Environ. Sci.
1222 Technol., 39, 4938–4952, 2005.
1223 Zhang, Q., Jimenez, J. L., Canagaratna, M. R. et al.: Ubiquity and dominance of
1224 oxygenated species in organic aerosols in anthropogenically influenced Northern
1225 Hemisphere midlatitudes, Geophys. Res. Lett., 34, L13801,

1226 doi:10.1029/2007GL029979, 2007.

1227

1228

1229 **Author's addresses**

1230 J. D. Fast, Atmospheric Science and Global Change Division, Pacific Northwest National
1231 Laboratory, MSINK9-30, P.O. Box 999, Richland, WA 99352, USA.
1232 (jerome.fast@pnnl.gov)
1233 Y. Kanaya, H. Matsui, and M. Takigawa, Research Institute for Global Change, Japan
1234 Agency for Marine-Earth Science and Technology, 3173-25, Showa-machi,
1235 Kanazawa-ku, Yokohama, Kanagawa, 236-0001, Japan. (yugo@jamstec.go.jp,
1236 matsui@jamstec.go.jp, takigawa@jamstec.go.jp)
1237 M. Koike and Y. Kondo, Department of Earth and Planetary Science, Graduate School of
1238 Science, The University of Tokyo, Hongo 7-3-1, Bunkyo-ku, Tokyo, 113-0033,
1239 Japan. (koike@eps.s.u-tokyo.ac.jp, kondo@eps.s.u-tokyo.ac.jp)
1240 A. Takami, National Institute for Environmental Studies, Onogawa 16-2, Tsukuba,
1241 Ibaraki 305-8506, Japan. (takamia@nies.go.jp)
1242
1243

Figure Captions

Fig. 1. Summary of the volatility basis-set approach used in this study. Circles and squares show individual gas-phase (open) and aerosol-phase (closed) surrogate species. Squares denote primary emission species. AN, BB, and BIO denote anthropogenic, biomass burning, and biogenic sources, respectively. The oxidation processes shown by black arrows are calculated with the coefficients given by Tsimipidi et al. (2010). The oxidation process shown by orange arrows are calculated assuming OH oxidation with the rate coefficient of 1×10^{-11} cm^{-3} $molecule^{-1}$ s^{-1}.

Fig. 2. Simulation domains (a) in and around Tokyo during the IMPACT campaign and (b) over East Asia during the A-FORCE campaign. (a) Simulations were conducted for 17 July to 15 August 2003 (IMPACT-2) and for 23 July to 15 August 2004 (IMPACT-L) with horizontal resolutions of 27 km (outer domain, orange) and 9 km (inner domain, red). Light blue squares show the locations of measurement stations at Komaba (35.66°N, 139.67°E) and Kisai (36.08°N, 139.55°E). (b) Simulations were conducted for 21 March to 26 April 2009 with horizontal resolutions of 180 km (outer domain, orange) and 60 km (inner domain, red). Light blue squares show the locations of measurement stations at Fukue (32.75°N, 128.68°E) and Kisai (26.87°N, 128.25°E).

Fig. 3. Period-averaged (24 March – 26 April 2009) emissions for (a) POA from anthropogenic sources (fossil fuel and biofuel combustion), (b) POA from biomass burning sources, (c) ARO1 (aromatics), and (d) TERP (monoterpenes). We used the anthropogenic and volcanic emission inventories of Streets et al.

(2003), daily biomass burning emissions of the Global Fire Emissions Database version 3 (GFED3) (van der Werf et al., 2010), and on-line biogenic emissions of the Model of Emissions of Gases and Aerosols from Nature version 2 (MEGAN2) (Guenther et al., 2006).

Fig. 4. Time series of observed and simulated (a) O_3 volume mixing ratio and (b) SOA mass concentrations at Kisai during the IMPACT-L campaign. SOA values were simulated with and without aging.

Fig. 5. Correlation of SOA mass concentrations with O_3 volume mixing ratio (a) at Komaba during the IMPACT-2 campaign and (b) at Kisai during the IMPACT-L campaign. Solid lines show fitting slopes (y = ax) for observation (blue) and simulations with (red) and without (orange) aging processes of organic vapors.

Fig. 6. Time series of (a, b) black carbon mass concentrations, (c, d) sulfate mass concentrations, (e, f) organic aerosol mass concentrations, and (g, h) organic to sulfate mass concentration ratios at Fukue and Hedo, respectively. Red shading in panels e and f shows the range of organic aerosol mass concentrations with the aging coefficient between 4×10^{-11} cm^3 $molecule^{-1}$ s^{-1} (4 times the base case) and 2.5×10^{-12} cm^3 $molecule^{-1}$ s^{-1} (1/4 times the base case). The periods when observed sulfate mass concentrations were less than 1 μg m^{-3} are not shown for measurements (blue points) in panels g and h.

Fig. 7. Period-averaged (24 March – 26 April 2009) simulated mass concentrations of POA (a, b), OPOA (c, d), ASOA (e, f), BSOA (g, h), and total SOA (sum of OPOA, ASOA, and BSOA) (i, j) at an altitude of about 1 km (layer number of 8, sigma level of 0.895). Left panels (a, c, e, g, i) are runs with aging, and right

1290 panels (b, d, f, h, j) are runs without aging.

1291 Fig. 8. Period-averaged (24 March – 26 April 2009) mass concentrations of POA,
1292 OPOA, ASOA, and BSOA at an altitude of about 1 km over the outer domain
1293 for Aging-on, Aging-off, Aging-bio, and Aging-an simulations (a). Period-
1294 averaged fraction of POA, OPOA, ASOA, and BSOA to total OA mass
1295 concentrations at an altitude of about 1 km over the outer domain for simulations
1296 with (b) or without (c) aging.

1297 Fig. 9. Diagram of sensitivity simulations conducted in Sect. 5. OA contributions
1298 estimated from individual simulations are shown. AVOC and BVOC denote
1299 anthropogenic and biogenic OVOCs, respectively.

1300 Fig. 10. Sensitivity of POA, OPOA, ASOA, and BSOA mass concentrations to changes
1301 in anthropogenic emissions (CO, NO_x, SO_2, VOCs, S/IVOCs, POA and BC) at
1302 an altitude of about 1 km over the outer domain. Mass concentrations and
1303 anthropogenic emissions in the sensitivity simulations are normalized by those
1304 in the base case simulation.

1305 Fig. 11. Period-averaged (24 March – 26 April 2009) fraction of controllable and non-
1306 controllable OA mass concentrations at an altitude of about 1 km over the outer
1307 domain for simulations with (a) or without (b) aging. Period-averaged (24
1308 March – 26 April 2009) fraction of controllable OA at an altitude of about 1 km
1309 over the outer domain for the simulation with aging (c).

1310

Table 1. Abbreviations for organic vapors and aerosols used in this study

Abbreviation	Definition	Explanation
OA	Organic aerosol	---
POA	Primary OA	Primary emission or formed from S/IVOCs by equilibrium (w/o oxidation)
SOA	Secondary OA	Sum of OPOA, BSOA, and ASOA
VOCs	Volatile organic compounds	Primary emission
S/IVOCs	Semi-volatile and intermediate volatility organic compounds	Primary emission (primary S/IVOCs) or secondary production through the oxidation of primary S/IVOCs (oxygenated S/IVOCs)
OVOCs	Oxygenated volatile organic compounds	Oxidation products of VOCs
HOA	Hydrocarbon-like OA	Obtained by AMS
OOA	Oxygenated OA	Obtained by AMS
OPOA	Oxygenated POA	OA formed from oxygenated S/IVOCs
BSOA	Biogenic SOA	OA formed from biogenic OVOCs
ASOA	Anthropogenic SOA	OA formed from anthropogenic OVOCs (including biomass burning sources)

Table 2. Meteorological and chemical process options used in this study

Atmospheric Process	Model Option
Longwave radiation	RRTM
Shortwave radiation	Goddard
Surface layer	Monin-Obukhov
Land surface	Noah
Boundary layer	YSU
Cumulus clouds	Kain-Fritsch
Cloud microphysics	Morrison
Gas-phase chemistry	SAPRC99
Aerosol nucleation	Binary nucleation
Aerosol condensation	MOSAIC
Aerosol coagulation	COAGSOLV
Aqueous-phase chemistry	Fahey and Pandis
Photolysis	Fast-J

Table 3. Summary of the VBS schemes developed in this study and original WRF-chem/MOSAIC model

Item/Process	This Study	Shrivastava et al. (2011)
Gas-phase chemistry	SAPRC99	SAPRC99
VBS volatility species	9 for POA and primary S/IVOCs 8 for OPOA and oxygenated S/IVOCs 4 for ASOA, BSOA, and OVOCs	9 for POA and primary S/IVOCs 8 for OPOA and oxygenated S/IVOCs 4 for ASOA, BSOA, and OVOCs
Oxidation species	VOCs, S/IVOCs, and OVOCs	VOCs and S/IVOCs
OVOCs formation	NO_x-dependent 4-product fit (Tsimpidi et al., 2010)	NO_x-dependent 4-product fit (Tsimpidi et al., 2010)
Gas-particle partitioning	Bulk equilibrium (Schell et al., 2001)	Bulk equilibrium (Donahue et al., 2006)
OA distribution to each size bin	Koo et al. (2003)	Koo et al. (2003)
Number of size bin	8 (40 – 10000 nm)	4 (40 – 10000 nm)
Number of variables in VBS	122 Gas-phase: 53 Bulk aerosol: 53 Size-resolved aerosol: 16 (interstitial aerosol, in-cloud aerosol)	380 Gas-phase: 76 Size-resolved aerosol: 304
Dry deposition	On	On
Aerosol activation	On	Off
Wet deposition	On	Off

Table 4. List of model simulations

Simulation	Aging coefficient (cm^3 $molucule^{-1}$ s^{-1})	
	S/IVOCs and anthropogenic OVOCs	Biogenic OVOCs
Aging-on	1e-11	1e-11
Aging-off	0	0
Aging-an	1e-11	0
Aging-bio	0	1e-11
Aging-0.25	2.5e-12	2.5e-12
Aging-4	4e-11	4e-11

Table 5. Statistics of concentrations of chemical species at the surface measurement sites

Station	Period	Species	Units	Mean concentration			NMB (%) [b]	R [b]
				Observation	Calculation [a] (Aging-on)	Calculation [a] (Aging-off)		
Komaba	19 July – 13 August 2003 (IMPACT-2)	O_3	ppbv	19.6	15.3	15.4	-22.3	0.63
		SOA	$\mu g\ m^{-3}$	4.36	3.45	1.03	-20.8	0.52
Kisai	25 July – 14 August 2004 (IMPACT-L)	O_3	ppbv	26.4	20.6	20.7	-21.9	0.84
		SOA	$\mu g\ m^{-3}$	5.31	4.61	0.76	-13.1	0.70
Fukue	27 March – 26 April 2009	BC	$\mu g\ m^{-3}$	0.87	0.75	0.74	-14.2	0.76
		SO_4	$\mu g\ m^{-3}$	9.31	8.29	8.27	-10.9	0.65
		OA	$\mu g\ m^{-3}$	6.02	6.75	0.71	12.2	0.34
		OA/SO_4	---	0.89	0.78	0.13	-11.9	0.28
Hedo	24 March – 26 April 2009	BC	$\mu g\ m^{-3}$	0.36	0.27	0.27	-24.3	0.46
		SO_4	$\mu g\ m^{-3}$	2.36	4.20	4.24	78.0	0.34
		OA	$\mu g\ m^{-3}$	1.08	1.99	0.18	84.2	0.25
		OA/SO_4	---	0.58	0.42	0.058	-29.7	0.58

[a] Values are calculated for the periods when measurements are available.

[b] Statistics are calculated for the Aging-on simulation.

Table 6. Period-averaged organic aerosol mass concentration (μg m^{-3}) in the boundary layer (~ 1 km) over the outer domain

Simulation	POA	OPOA	ASOA	BSOA	Total OA
Aging-on	0.236	0.369	0.333	0.346	1.284
Aging-off	0.164	0.000	0.023	0.048	0.236
Aging-an	0.229	0.357	0.313	0.111	1.004
Aging-bio	0.196	0.000	0.038	0.241	0.474
Aging-0.25	0.188	0.056	0.106	0.132	0.483
Aging-4	0.275	1.223	0.661	0.654	2.813
Aging-on (an off) [a]	0.047	0.035	0.007	0.075	0.165
Aging-off (an off) [a]	0.040	0.000	0.001	0.018	0.059

[a] Simulations without anthropogenic emissions (with biomass burning, biogenic, and volcanic emissions).

Fig. 1

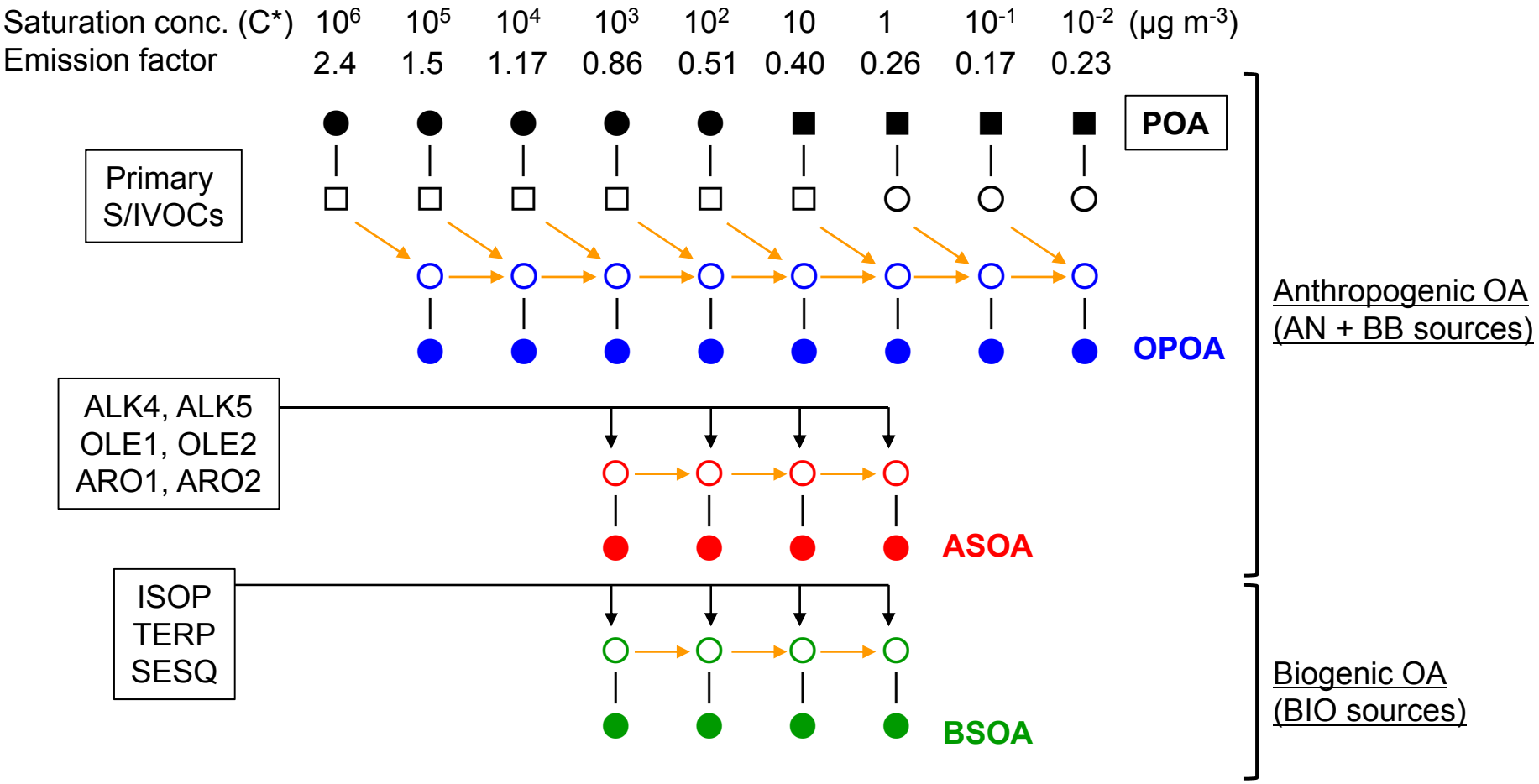
Saturation conc. (C*) 10^6 10^5 10^4 10^3 10^2 10 1 10^-1 10^-2 (µg m^-3)
Emission factor 2.4 1.5 1.17 0.86 0.51 0.40 0.26 0.17 0.23
POA
Primary S/IVOCs
OPOA
ALK4, ALK5 OLE1, OLE2 ARO1, ARO2
ASOA
ISOP TERP SESQ
BSOA
Anthropogenic OA (AN + BB sources)
Biogenic OA (BIO sources)

Fig. 2

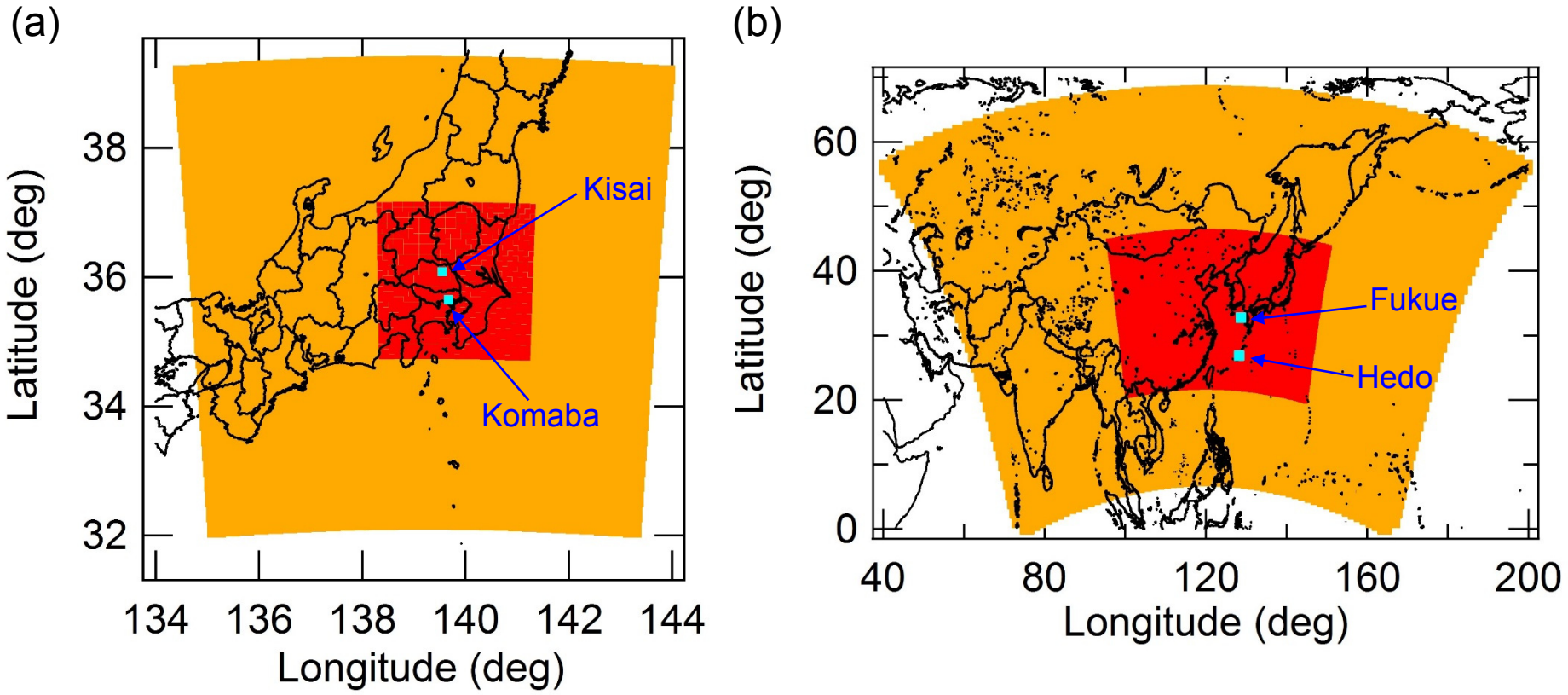
(a)
Kisai
Komaba
38
36
34
32
134
136
138
140
142
144
Latitude (deg)
Longitude (deg)
(b)
Fukue
Hedo
60
40
20
0
40
80
120
160
200
Latitude (deg)
Longitude (deg)

Fig. 3

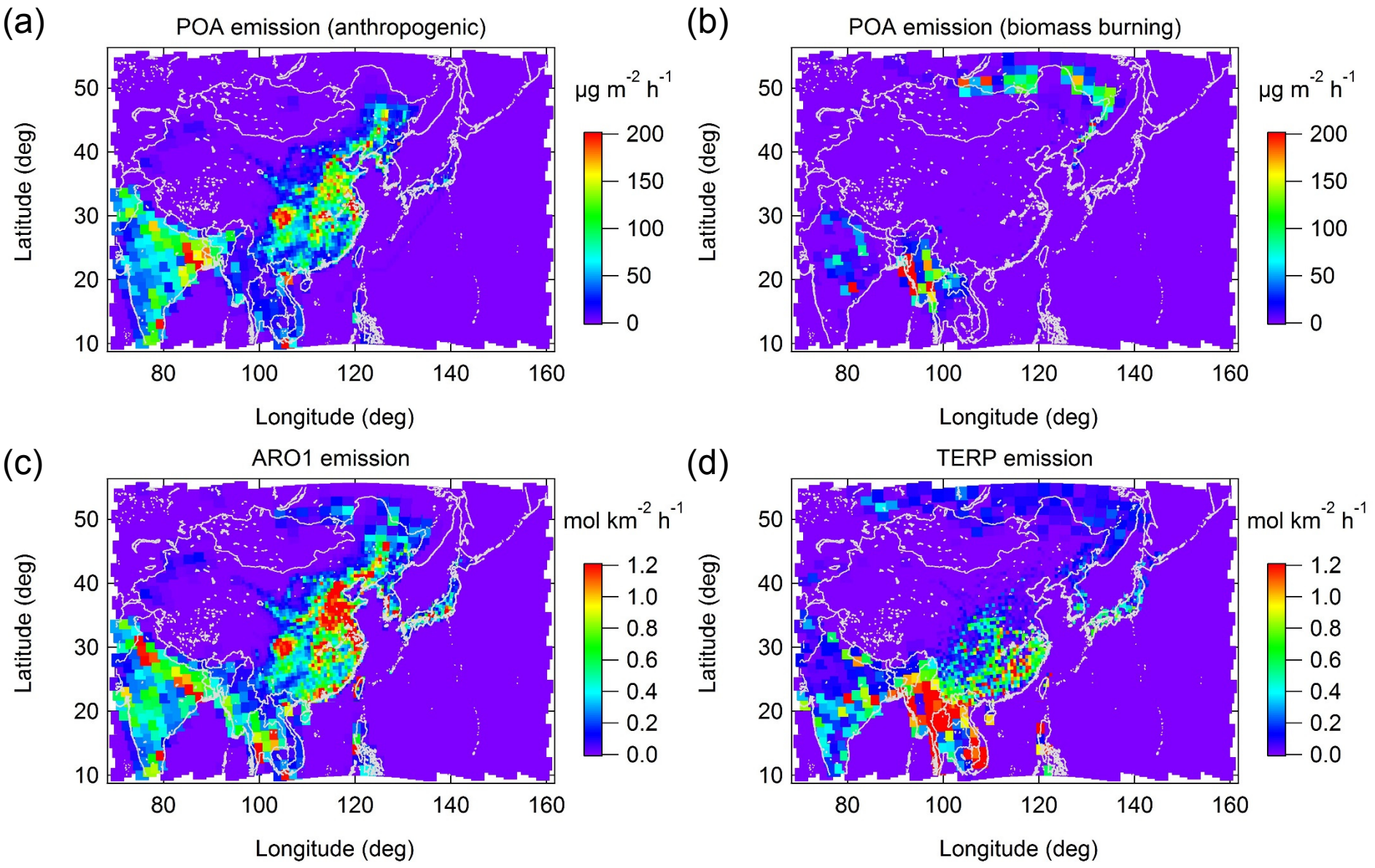
(a)
POA emission (anthropogenic)
μg m-2 h-1
200
150
100
50
0
Latitude (deg)
Longitude (deg)
10
20
30
40
50
80
100
120
140
160
(b)
POA emission (biomass burning)
μg m-2 h-1
200
150
100
50
0
Latitude (deg)
Longitude (deg)
(c)
ARO1 emission
mol km-2 h-1
1.2
1.0
0.8
0.6
0.4
0.2
0.0
Latitude (deg)
Longitude (deg)
(d)
TERP emission
mol km-2 h-1
1.2
1.0
0.8
0.6
0.4
0.2
0.0
Latitude (deg)
Longitude (deg)

Fig. 4

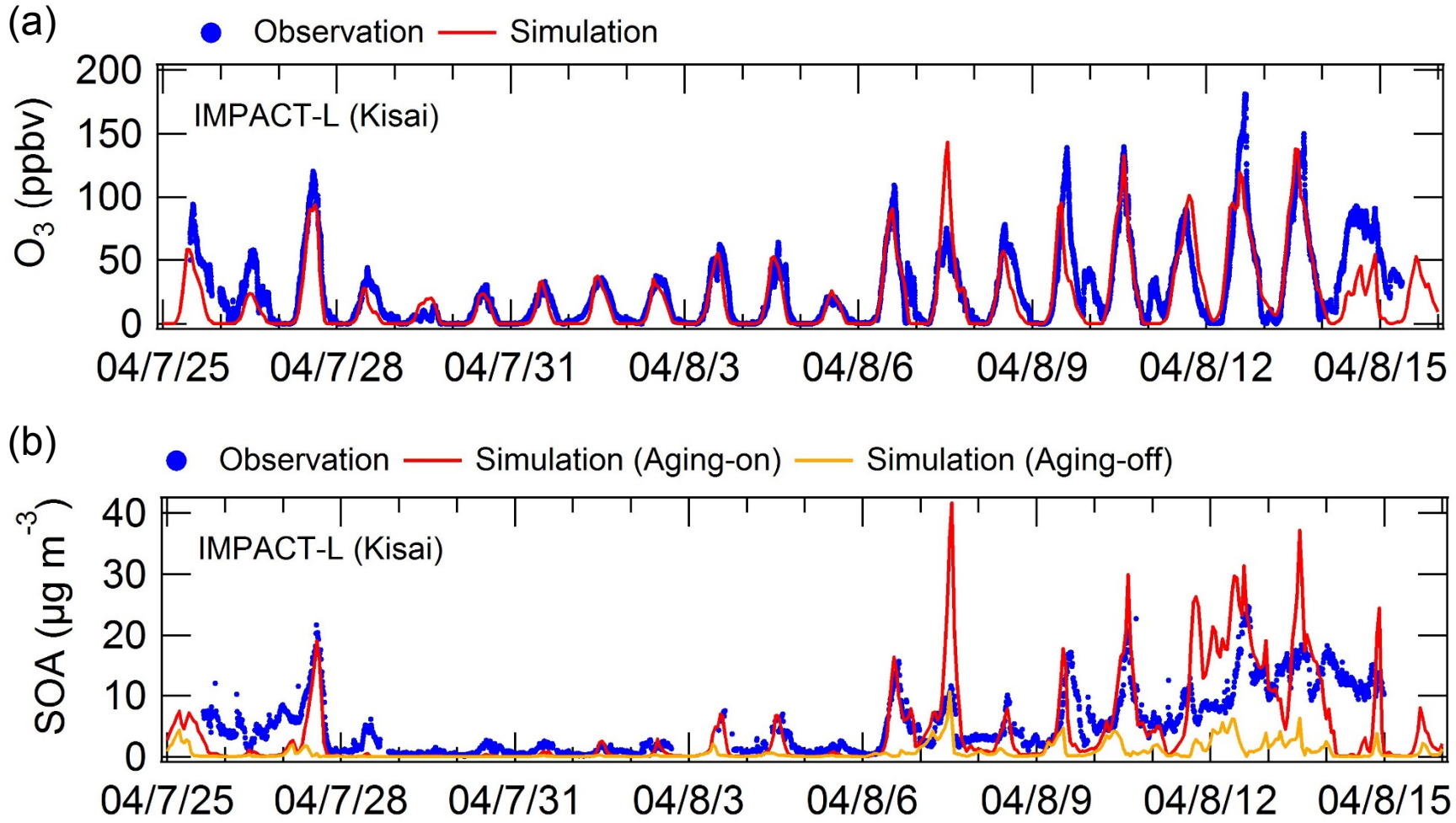
(a)
Observation
Simulation
IMPACT-L (Kisai)
O_3 (ppbv)
200
150
100
50
0
04/7/25
04/7/28
04/7/31
04/8/3
04/8/6
04/8/9
04/8/12
04/8/15
(b)
Observation
Simulation (Aging-on)
Simulation (Aging-off)
IMPACT-L (Kisai)
SOA (μg m^{-3})
40
30
20
10
0
04/7/25
04/7/28
04/7/31
04/8/3
04/8/6
04/8/9
04/8/12
04/8/15

Fig. 5

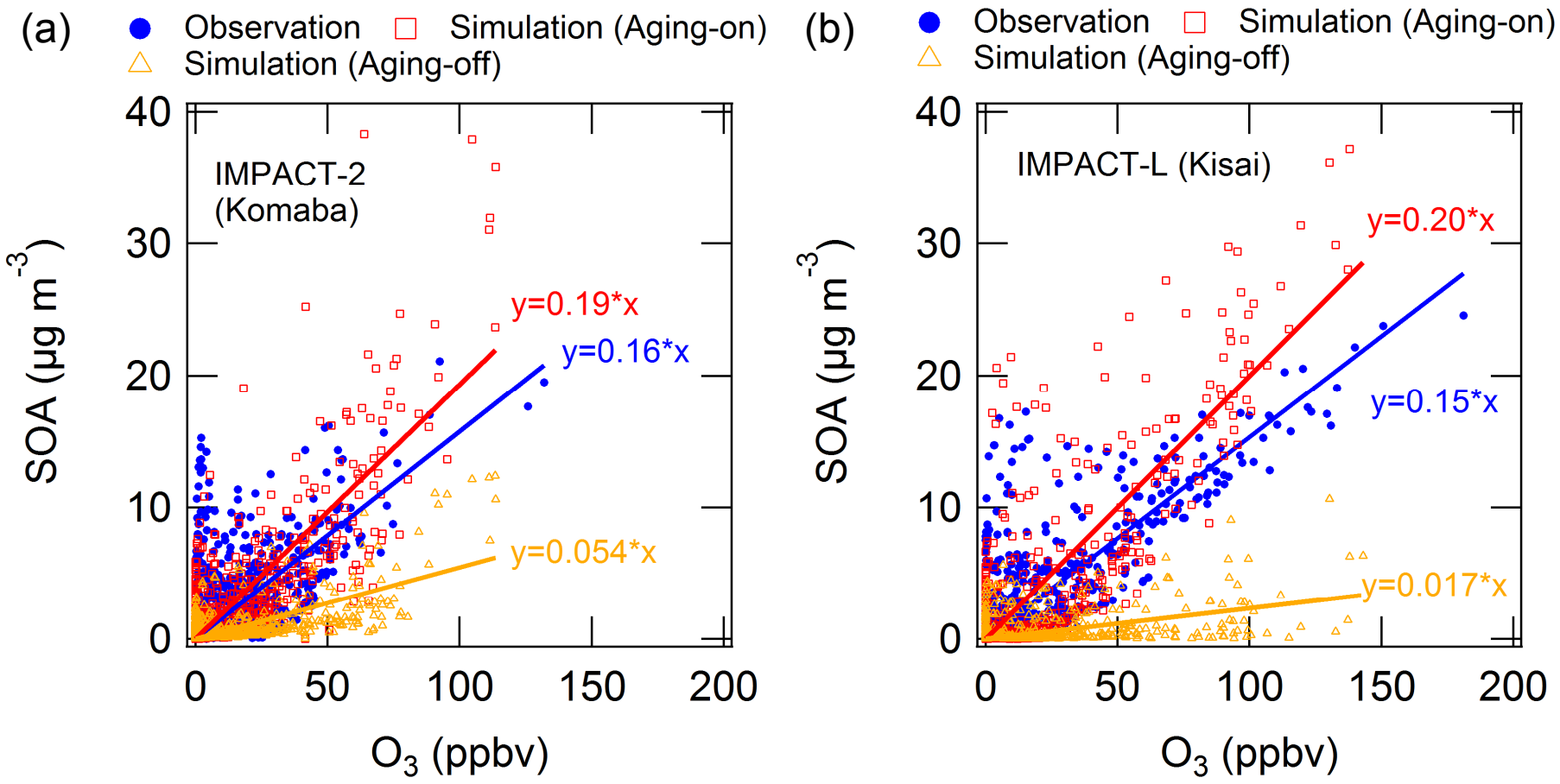
(a)
Observation
Simulation (Aging-on)
Simulation (Aging-off)
IMPACT-2
(Komaba)
y=0.19*x
y=0.16*x
y=0.054*x
SOA (μg m-3)
O3 (ppbv)
0
10
20
30
40
0
50
100
150
200
(b)
Observation
Simulation (Aging-on)
Simulation (Aging-off)
IMPACT-L (Kisai)
y=0.20*x
y=0.15*x
y=0.017*x
SOA (μg m-3)
O3 (ppbv)

Fig. 6

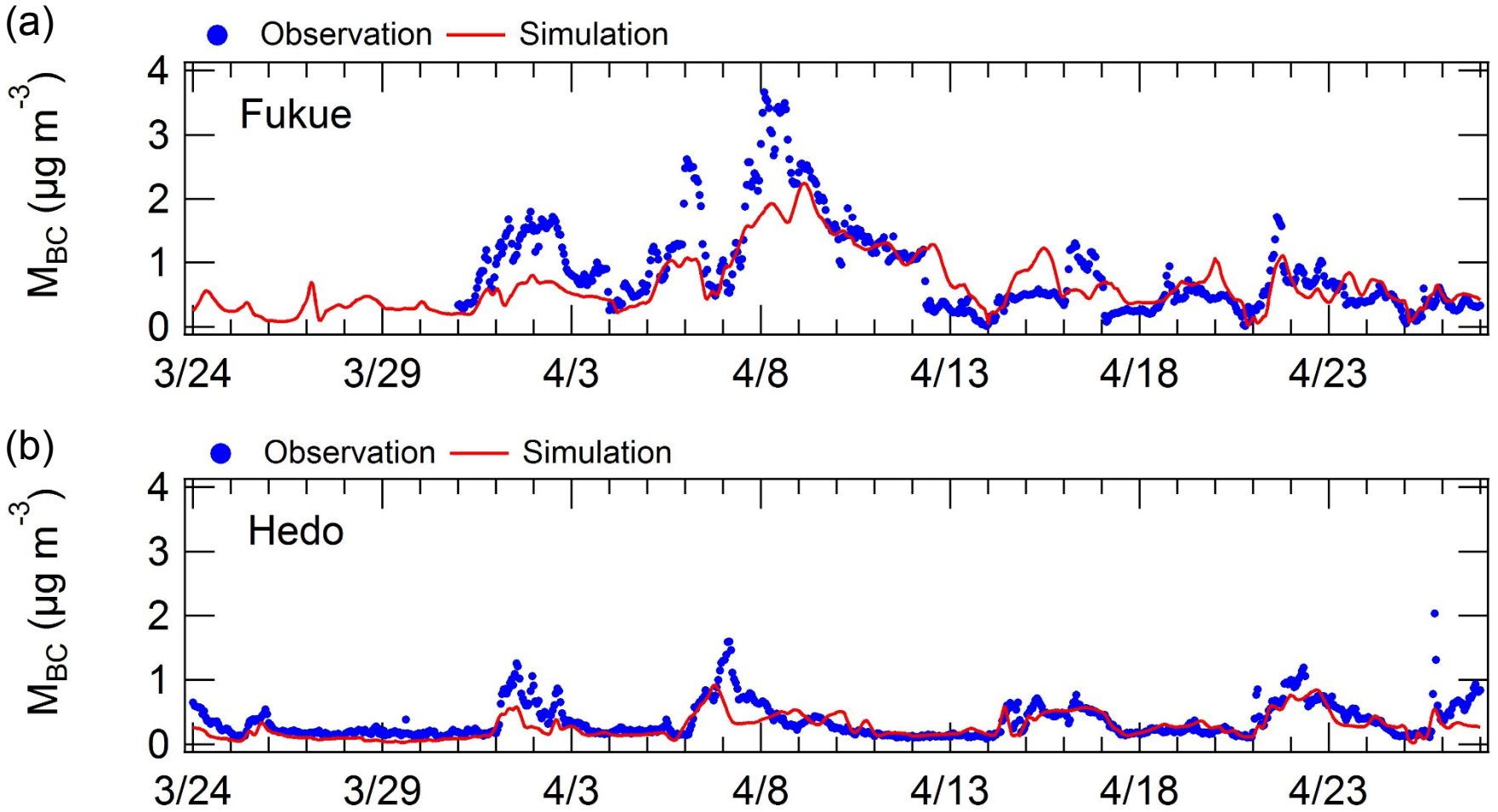
(a)
Observation
Simulation
Fukue
M_{BC} ($\mu g\ m^{-3}$)
0
1
2
3
4
3/24
3/29
4/3
4/8
4/13
4/18
4/23
(b)
Observation
Simulation
Hedo
M_{BC} ($\mu g\ m^{-3}$)
0
1
2
3
4
3/24
3/29
4/3
4/8
4/13
4/18
4/23

Fig. 6 (cont.)

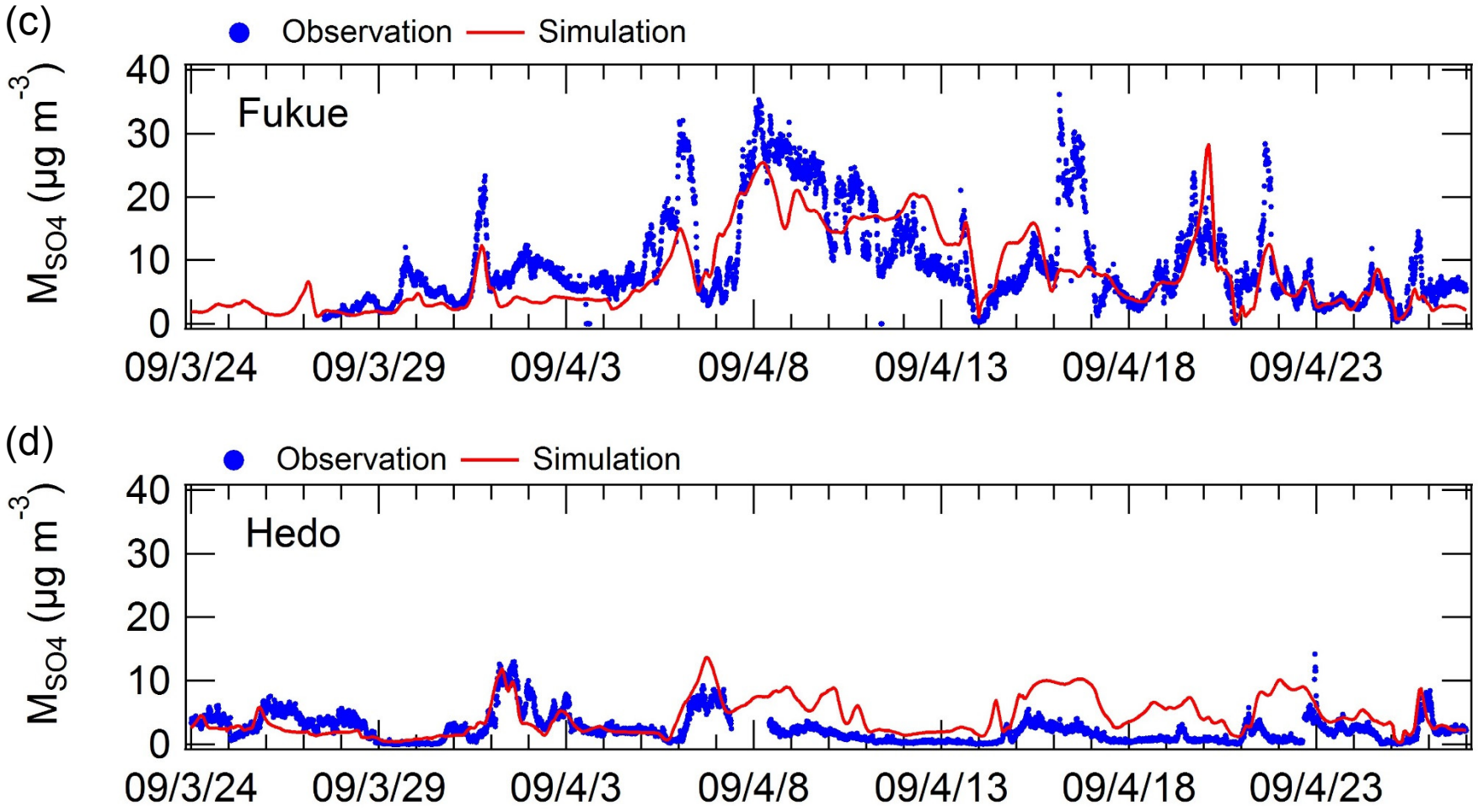
(c)
Observation
Simulation
Fukue
M_{SO4} (μg m^{-3})
40
30
20
10
0
09/3/24
09/3/29
09/4/3
09/4/8
09/4/13
09/4/18
09/4/23
(d)
Observation
Simulation
Hedo
M_{SO4} (μg m^{-3})
40
30
20
10
0
09/3/24
09/3/29
09/4/3
09/4/8
09/4/13
09/4/18
09/4/23

Fig. 6 (cont.)

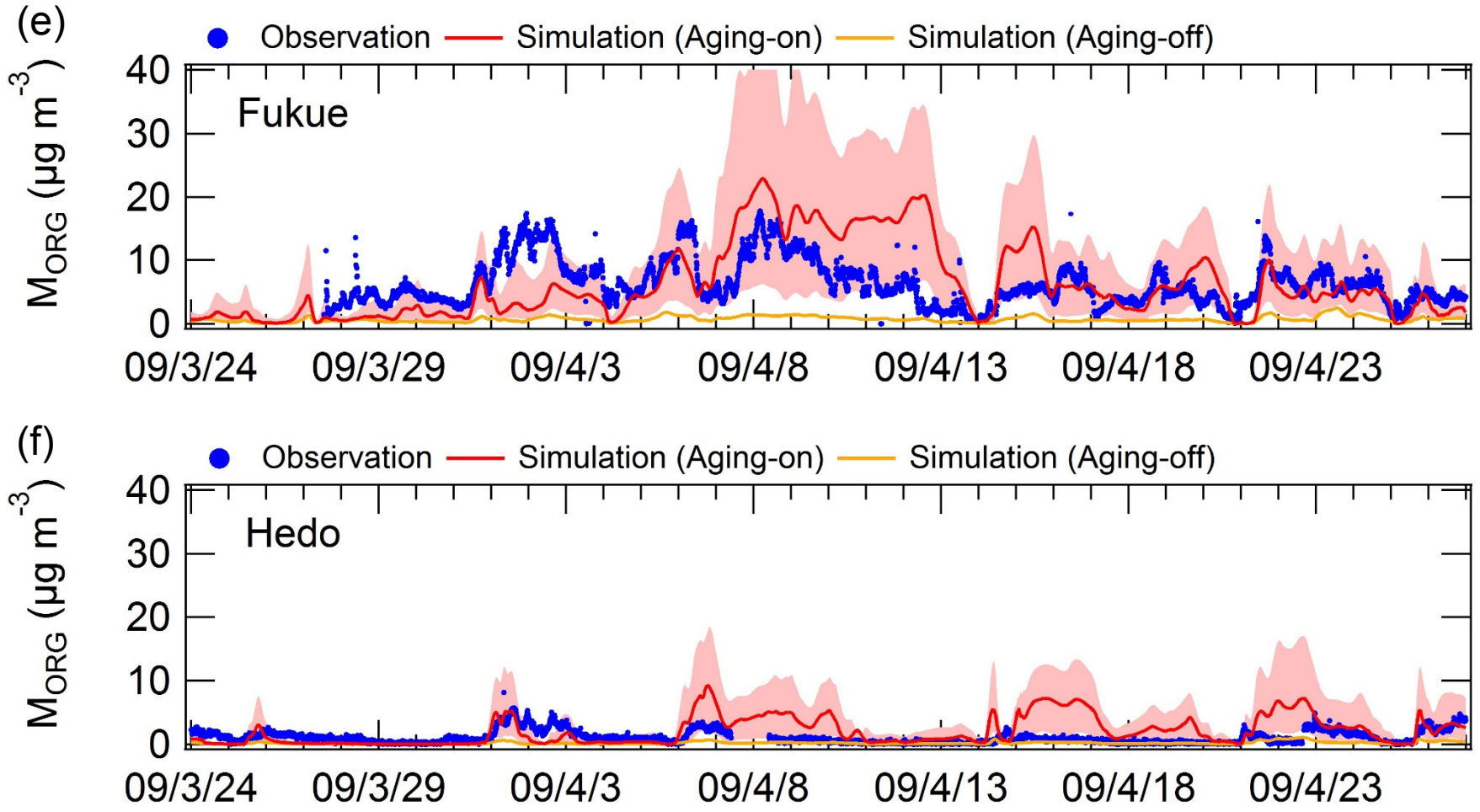
(e)
Observation
Simulation (Aging-on)
Simulation (Aging-off)
Fukue
M_{ORG} (μg m^{-3})
40
30
20
10
0
09/3/24
09/3/29
09/4/3
09/4/8
09/4/13
09/4/18
09/4/23
(f)
Observation
Simulation (Aging-on)
Simulation (Aging-off)
Hedo
M_{ORG} (μg m^{-3})
40
30
20
10
0
09/3/24
09/3/29
09/4/3
09/4/8
09/4/13
09/4/18
09/4/23

Fig. 6 (cont.)

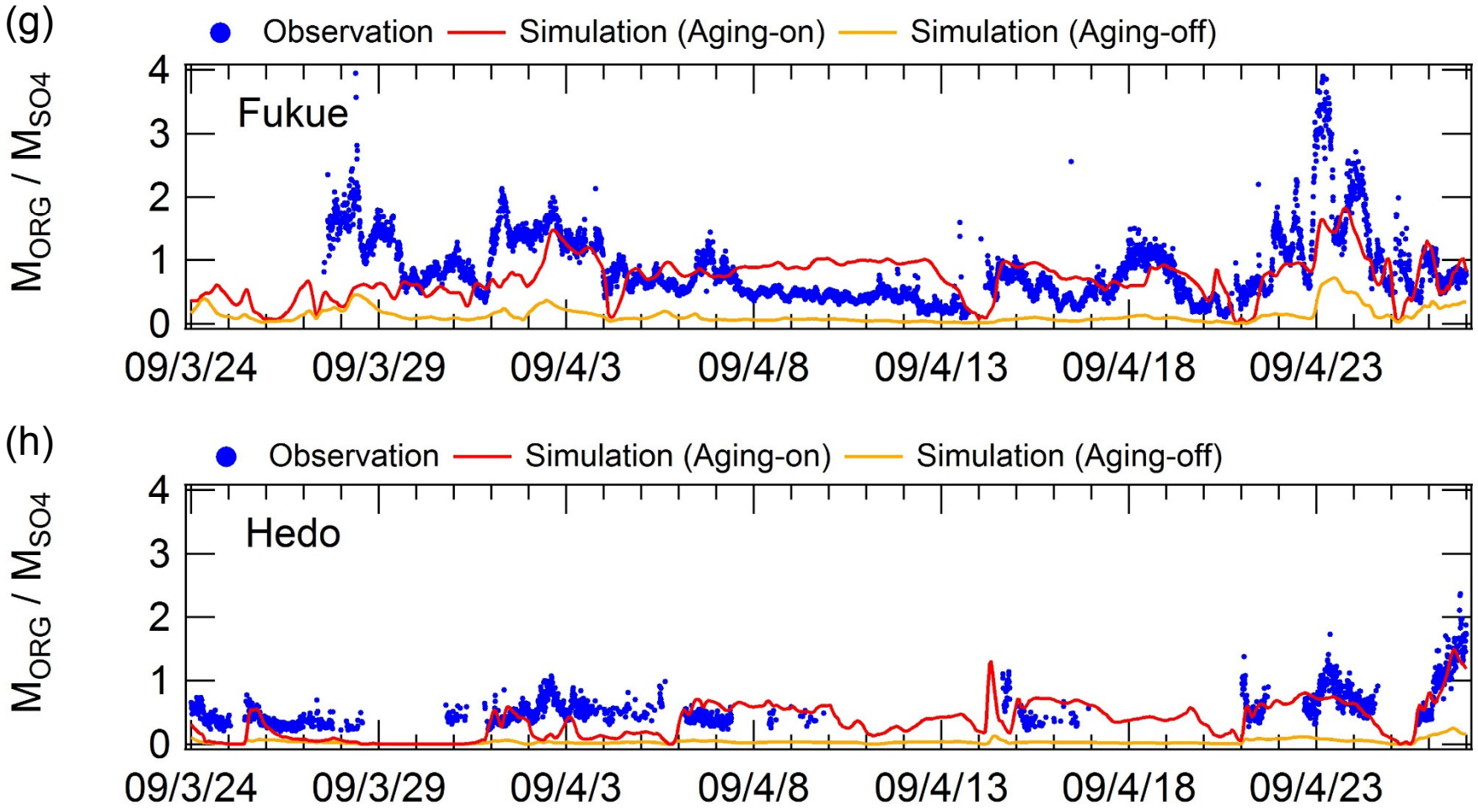
(g)
Observation
Simulation (Aging-on)
Simulation (Aging-off)
M_{ORG} / M_{SO4}
Fukue
0
1
2
3
4
09/3/24
09/3/29
09/4/3
09/4/8
09/4/13
09/4/18
09/4/23
(h)
Observation
Simulation (Aging-on)
Simulation (Aging-off)
M_{ORG} / M_{SO4}
Hedo
0
1
2
3
4
09/3/24
09/3/29
09/4/3
09/4/8
09/4/13
09/4/18
09/4/23

Fig. 7

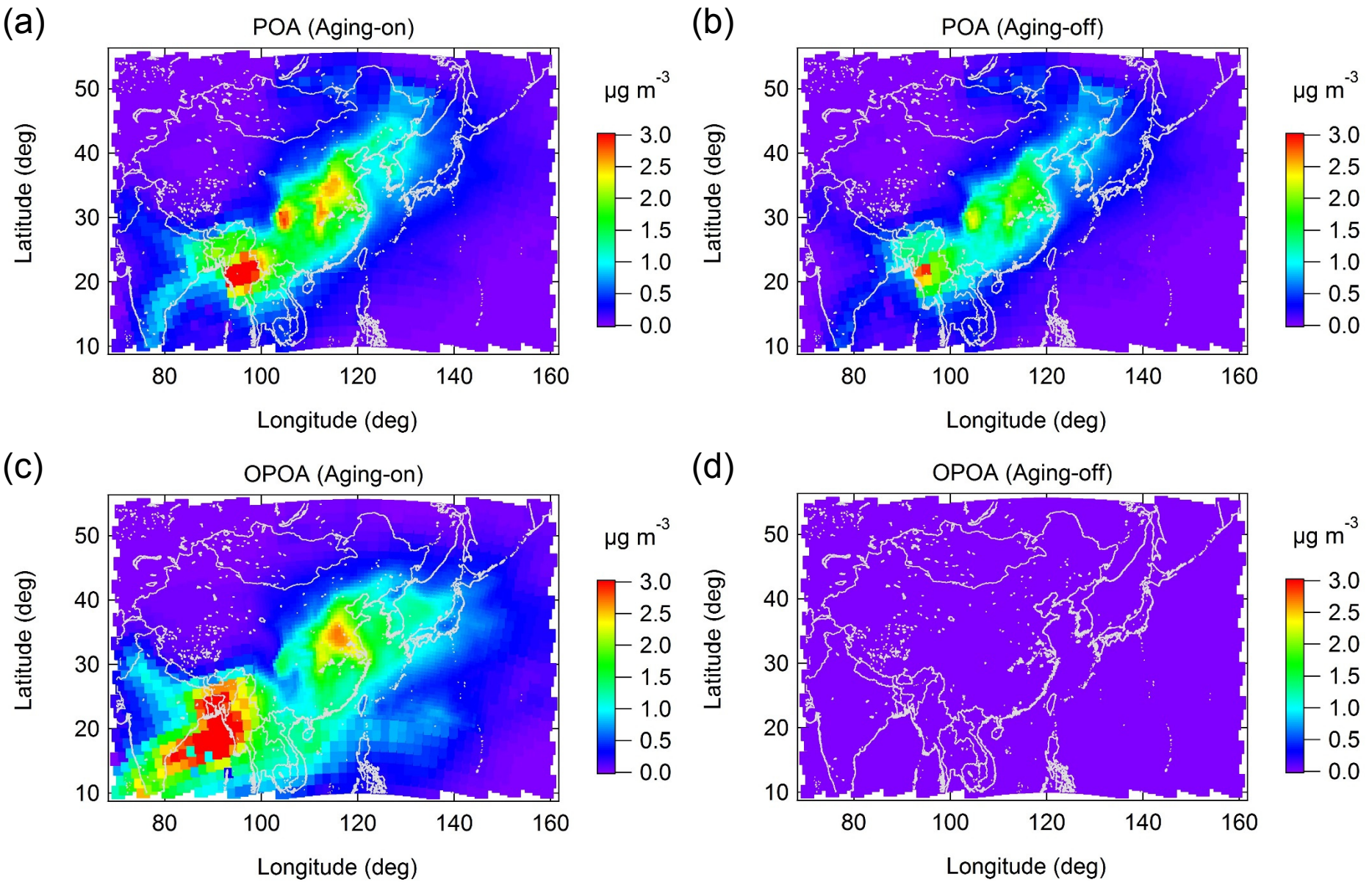
(a)
POA (Aging-on)
(b)
POA (Aging-off)
(c)
OPOA (Aging-on)
(d)
OPOA (Aging-off)
Latitude (deg)
Longitude (deg)
10
20
30
40
50
80
100
120
140
160
μg m-3
3.0
2.5
2.0
1.5
1.0
0.5
0.0

Fig. 7 (cont.)

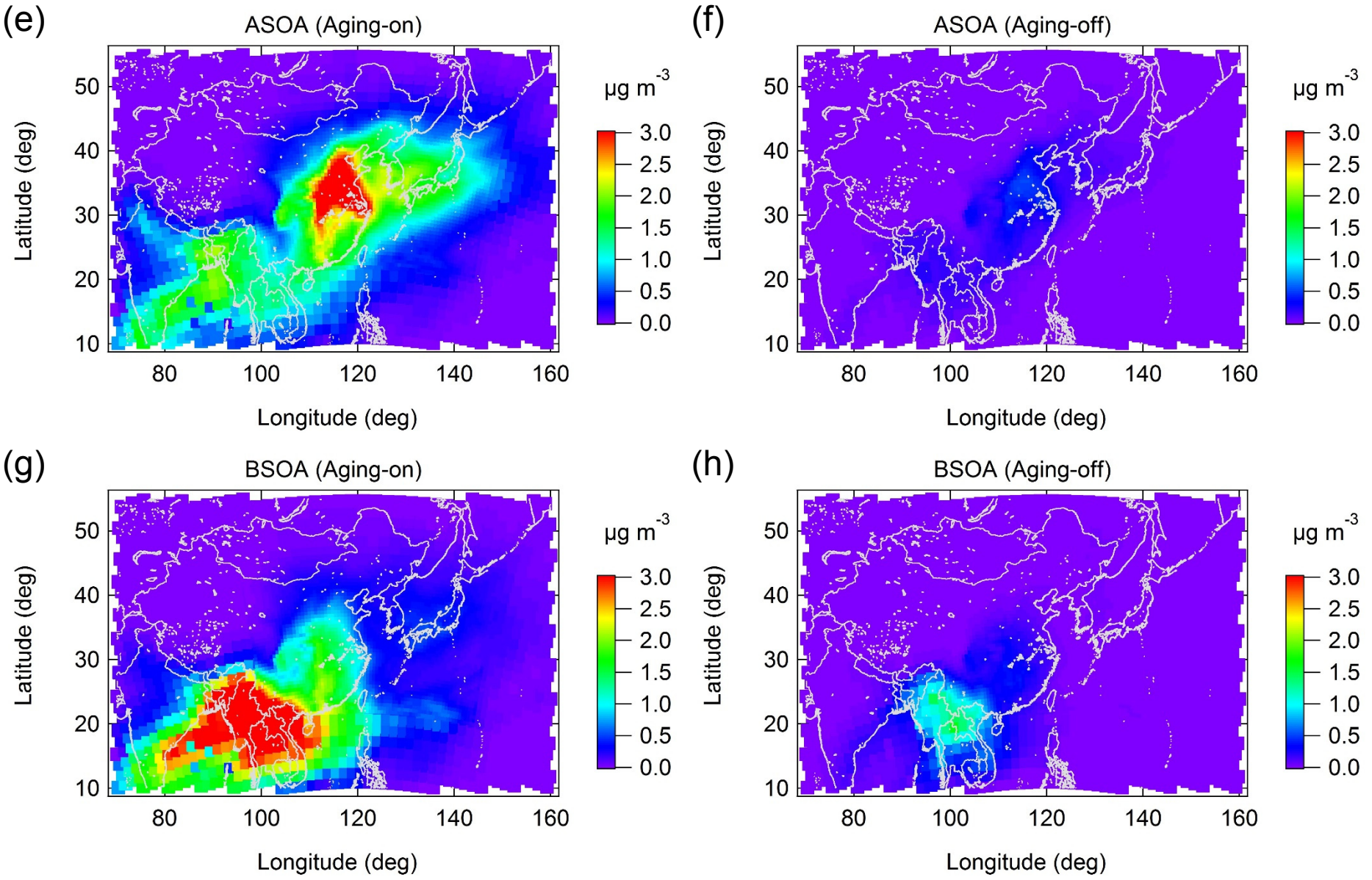
(e)
ASOA (Aging-on)
(f)
ASOA (Aging-off)
(g)
BSOA (Aging-on)
(h)
BSOA (Aging-off)
Latitude (deg)
Longitude (deg)
10
20
30
40
50
80
100
120
140
160
μg m-3
3.0
2.5
2.0
1.5
1.0
0.5
0.0

Fig. 7 (cont.)

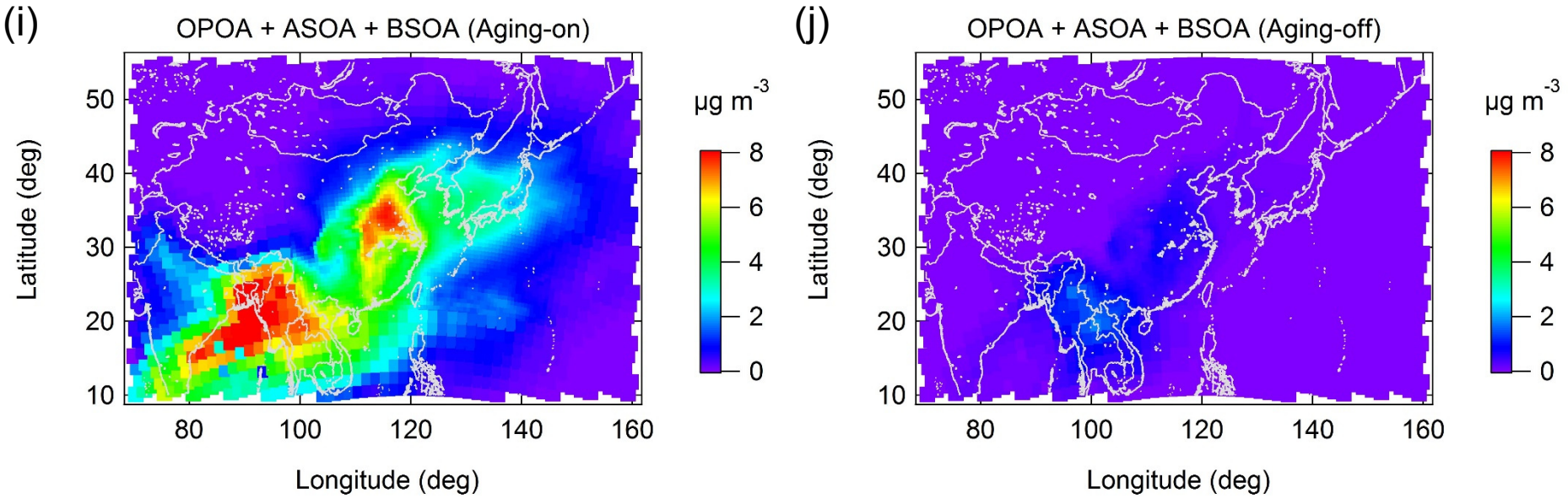
(i)
OPOA + ASOA + BSOA (Aging-on)
Latitude (deg)
Longitude (deg)
μg m-3
(j)
OPOA + ASOA + BSOA (Aging-off)
Latitude (deg)
Longitude (deg)
μg m-3

Fig. 8

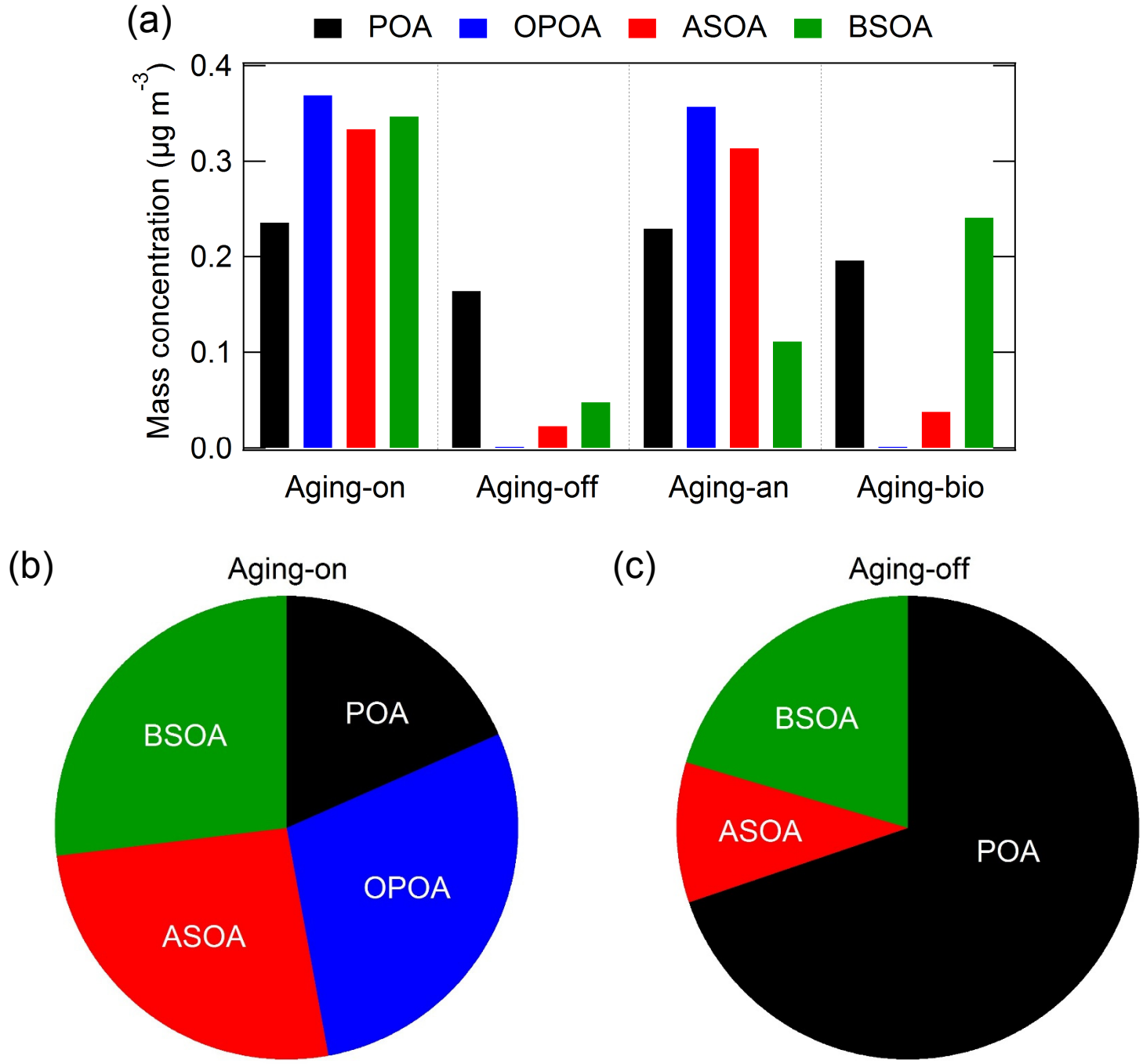
(a)
POA
OPOA
ASOA
BSOA
Mass concentration (μg m-3)
0.4
0.3
0.2
0.1
0.0
Aging-on
Aging-off
Aging-an
Aging-bio
(b)
Aging-on
BSOA
POA
OPOA
ASOA
(c)
Aging-off
BSOA
ASOA
POA

Fig. 9

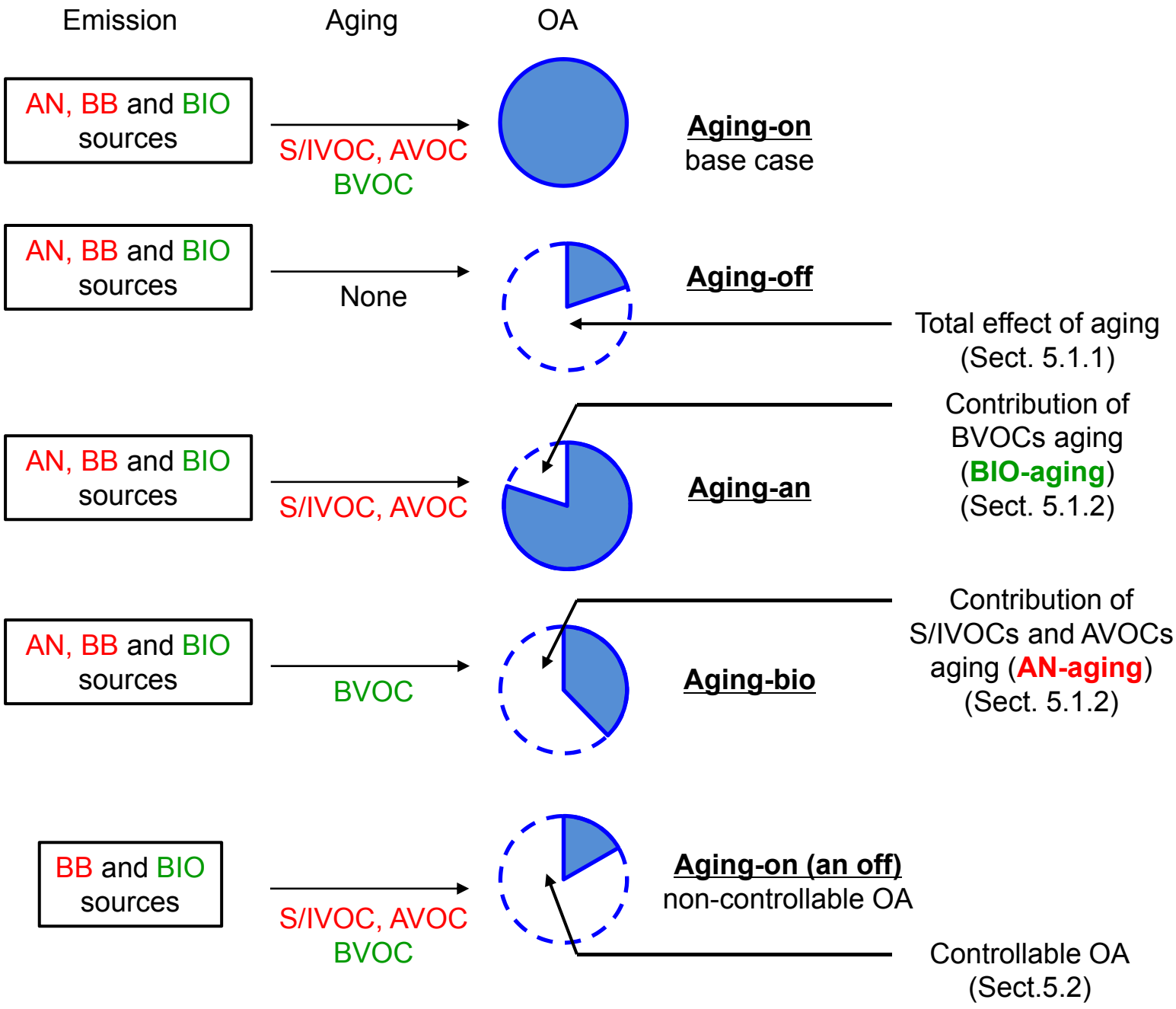
Emission
Aging
OA
AN, BB and BIO sources
S/IVOC, AVOC
BVOC
Aging-on
base case
AN, BB and BIO sources
None
Aging-off
Total effect of aging
(Sect. 5.1.1)
AN, BB and BIO sources
S/IVOC, AVOC
Aging-an
Contribution of BVOCs aging (BIO-aging) (Sect. 5.1.2)
AN, BB and BIO sources
BVOC
Aging-bio
Contribution of S/IVOCs and AVOCs aging (AN-aging) (Sect. 5.1.2)
BB and BIO sources
S/IVOC, AVOC
BVOC
Aging-on (an off)
non-controllable OA
Controllable OA
(Sect.5.2)

Fig. 10

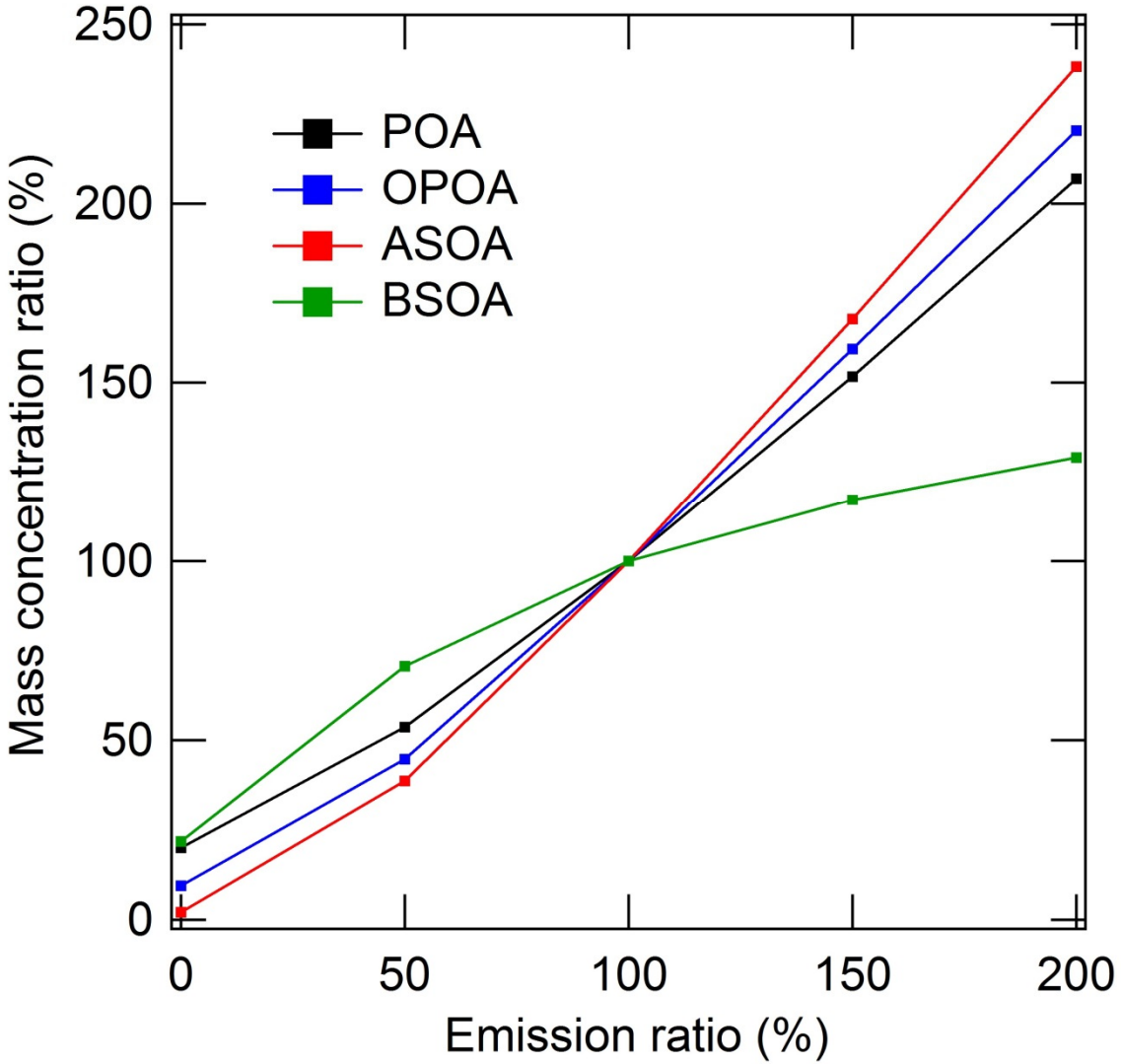
POA
OPOA
ASOA
BSOA
Mass concentration ratio (%)
Emission ratio (%)
0
50
100
150
200
250

Fig. 11

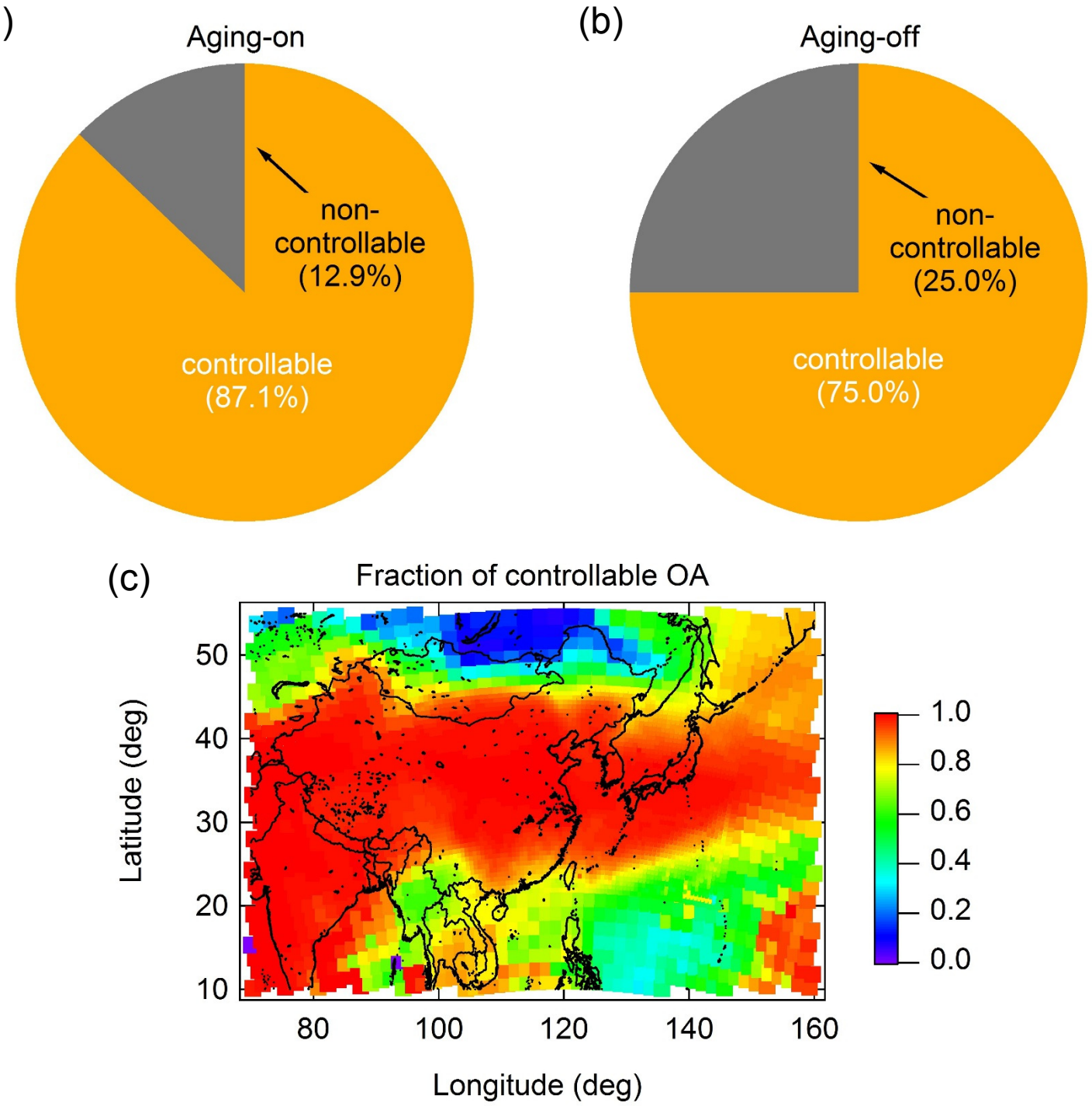
(a)
Aging-on
non-
controllable
(12.9%)
controllable
(87.1%)
(b)
Aging-off
non-
controllable
(25.0%)
controllable
(75.0%)
(c)
Fraction of controllable OA
Latitude (deg)
10
20
30
40
50
80
100
120
140
160
Longitude (deg)
1.0
0.8
0.6
0.4
0.2
0.0